Cell Reports

Article

Distinct mechanisms for sebaceous gland self-renewal and regeneration provide durability in response to injury

Graphical abstract

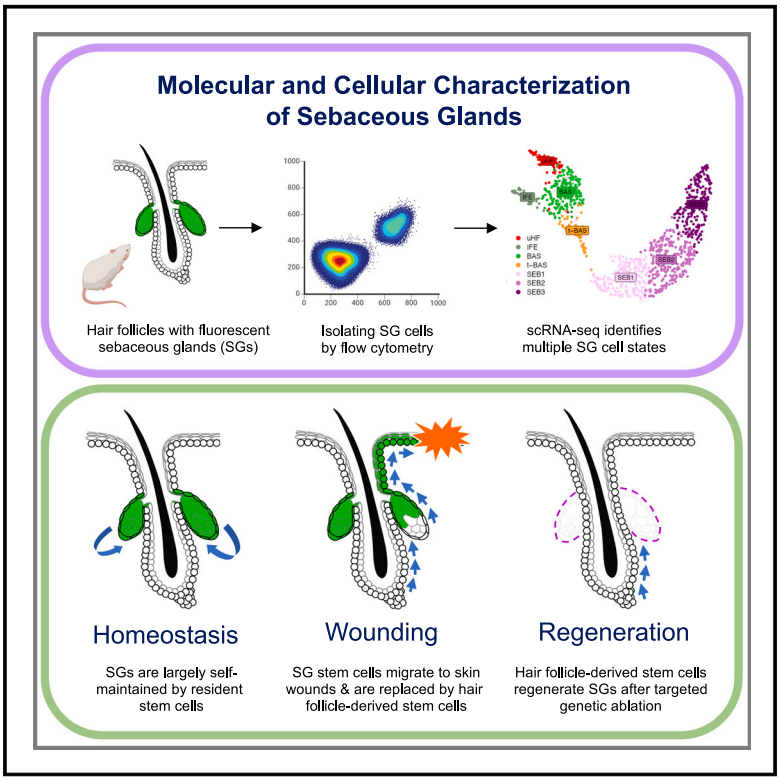

Highlights

- SGs are largely self-renewed by resident stem cells during homeostasis
- Alternative hair follicle stem cells regenerate the gland after ablation
- scRNA-seq identifies direct and indirect paths for sebocyte differentiation
- Transitional basal cells in the SG co-express Keratin 5 and PPARγ

Authors

Natalia A. Veniaminova, Yunlong Y. Jia, Adrien M. Hartigan, ..., Andrzej A. Dlugosz, Scott X. Atwood, Sunny Y. Wong

Correspondence

satwood@uci.edu (S.X.A.), sunnyw@umich.edu (S.Y.W.)

In brief

Veniaminova et al. characterize the development, maintenance, and regeneration of sebaceous glands (SGs). Although SGs are largely self-maintained by dedicated stem cells during homeostasis, alternative stem cells enter and regenerate the gland following injury. This regenerative process relies on FGF signaling and can be accelerated by stimulating hair growth.

Veniaminova et al., 2023, Cell Reports *42*, 113121
September 26, 2023
https://doi.org/10.1016/j.celrep.2023.113121

CellPress

Cell Reports

CellPress
OPEN ACCESS

Article

Distinct mechanisms for sebaceous gland self-renewal and regeneration provide durability in response to injury

Natalia A. Veniaminova,[1,5] Yunlong Y. Jia,[2,5] Adrien M. Hartigan,[1] Thomas J. Huyge,[1] Shih-Ying Tsai,[1] Marina Grachtchouk,[1] Seitaro Nakagawa,[3,4] Andrzej A. Dlugosz,[1] Scott X. Atwood,[2,*] and Sunny Y. Wong[1,6,*]

[1]Department of Dermatology, Department of Cell and Developmental Biology, University of Michigan, Ann Arbor, MI 48109, USA
[2]Department of Developmental and Cell Biology, University of California, Irvine, Irvine, CA 92697, USA
[3]Department of Pathology, University of Michigan, Ann Arbor, MI 48109, USA
[4]Department of Dermatology, Department of Cutaneous Immunology and Microbiology, Graduate School of Medicine, Osaka University, Suita, Osaka, 565-0871, Japan
[5]These authors contributed equally
[6]Lead contact
*Correspondence: satwood@uci.edu (S.X.A.), sunnyw@umich.edu (S.Y.W.)
https://doi.org/10.1016/j.celrep.2023.113121

SUMMARY

Sebaceous glands (SGs) release oils that protect our skin, but how these glands respond to injury has not been previously examined. Here, we report that SGs are largely self-renewed by dedicated stem cell pools during homeostasis. Using targeted single-cell RNA sequencing, we uncovered both direct and indirect paths by which resident SG progenitors ordinarily differentiate into sebocytes, including transit through a Krt5+PPARγ+ transitional basal cell state. Upon skin injury, however, SG progenitors depart their niche, re-epithelialize the wound, and are replaced by hair-follicle-derived stem cells. Furthermore, following targeted genetic ablation of >99% of SGs from dorsal skin, these glands unexpectedly regenerate within weeks. This regenerative process is mediated by alternative stem cells originating from the hair follicle bulge, is dependent upon FGFR2 signaling, and can be accelerated by inducing hair growth. Altogether, our studies demonstrate that stem cell plasticity promotes SG durability following injury.

INTRODUCTION

Our skin is coated with a complex mixture of oils that serves critical roles in modulating water retention, body temperature, and the microbiome. These oily secretions, known as sebum, originate from sebaceous glands (SGs) and constitute up to 90% of the total surface lipids in the skin.[1,2] Over-production of sebum by SGs can lead to "oily skin," whereas hyposecretion of sebum is often associated with dry skin and eczematous dermatoses.[3,4] Since perturbations in sebum are notably linked to common cutaneous disorders such as acne, seborrheic dermatitis, and enlarged facial pores, SGs must be exquisitely regulated in order to maintain healthy skin function and cosmetic appearance.[5,6]

SGs are epithelial appendages typically associated with hair follicles. These acinar structures are composed of terminally differentiated sebocytes ensheathed by a peripheral layer of undifferentiated basal progenitor cells.[7,8] During maturation, sebocytes enlarge, accumulate lipids, and degrade their organelles in a specialized form of cell death known as holocrine secretion.[9] This process culminates with sebocytes releasing their lipid contents through the sebaceous duct into the hair follicle infundibulum, which provides a passageway for sebum to exit the follicle and enter the skin surface.[10]

Since SGs are hormonally regulated, their activity varies at different stages of life.[11,12] Nonetheless, the constant turnover of sebocytes necessitates that these cells be continually replenished, a process that typically takes 1–2 weeks in mice and 2–4 weeks in humans.[13–16] This renewal process is made possible by stem cells, although the niche in which these cells reside has not been decisively established. Although some studies have noted that hair follicle stem cells can enter and renew the gland,[17–19] other reports have indicated that SGs harbor their own dedicated stem cell pools.[20–23] In addition, it remains controversial whether all basal progenitors that line the SG periphery contribute equally to sebocyte formation. Finally, whether these cellular processes become altered after injury has not been explored.

Technical challenges have posed a major hindrance to answering these questions. Because SGs are lobular structures that exhibit cellular heterogeneity along multiple axes—including proximal-distal, as well as proximity to the sebaceous duct—the spatial and molecular relationships of sebocytes at different stages of differentiation have been difficult to resolve. In addition, the lack of Cre drivers that specifically and efficiently target SGs complicates genetic fate mapping studies. Indeed, current tools for performing lineage tracing on SGs rely on mouse Cre

lines that also target the hair follicle.[18,22,24,25] Sebocytes are also challenging to isolate due to their complex cellular properties. Consequently, these cells typically constitute a minor sub-population in single-cell RNA sequencing (scRNA-seq) studies of skin, precluding the ability to perform deeper analyses.[26–28] Finally, studies on SG function have historically relied on mouse mutants such as *Asebia*, which possesses impaired SGs due to a germline mutation in *stearoyl-Coenzyme A desaturase-1* (*Scd1*).[29,30]

Recent reports have suggested that SGs are adaptable structures that respond to local and systemic cues, are affected by the hair cycle and immune factors, and appear to be lost in diseases such as cicatricial alopecia and psoriasis.[31–37] Here, we overcome many of the technical challenges for studying SGs and perform highly targeted genetic fate mapping, scRNA-seq, and ablation studies to explore how distinct stem cell populations maintain the gland and confer resiliency in response to injury.

RESULTS

Establishing SG landmarks

Keratins are by far the most abundant proteins in the skin, and the expression patterns of the 54 keratin family members subdivide keratinocytes by niche, function, and differentiation status.[38] We previously reported that basal progenitors at the SG periphery express keratins (K) 5 and K14, which form prototypic heterodimers in multiple mouse skin stem cell compartments (Figure 1A).[20] In differentiated sebocytes, however, K14 levels remain high, whereas expression of its typical binding partner K5 is reduced (Figure 1A). In its place, a different keratin, K79, becomes elevated in sebocytes and heterodimerizes with K14 (Figure 1B).[20] Therefore, SG progenitors undergo a K14:K5 → K14:K79 keratin switch when they become sebocytes. Whether other keratins display similar shifts in the SG remains unclear and will be examined below.

Notably, we also observed that peroxisome proliferator-activated receptor gamma (PPARγ), a master regulator of lipid metabolism and SG differentiation,[41,42] is initially expressed by K5+ basal SG progenitors located at the lower (proximal) region of the gland (Figure 1C). A subset of basal PPARγ+ cells are also proliferative (Figure 1D). Because these cells express a unique combination of both basal progenitor (K5) and differentiation (PPARγ) markers, this suggests that these K5+PPARγ+ cells may behave as transitional basal cells poised to differentiate into sebocytes, a concept we revisit later (Figure 1E).

To determine whether these expression patterns are recapitulated during initial SG development, we examined mouse embryonic skin after hair follicle initiation but before SG formation. We have previously shown that nascent hair buds generate and extend columns of K79+ differentiated cells out into the epidermis, which subsequently undergo remodeling to form hair follicle openings.[39,43] In embryonic (E) day 16.5 skin, we observed K79+ columns in developing hair buds, as expected, but no PPARγ expression (Figure 1F). By E17.5, however, we noticed basal PPARγ expression, reminiscent of the K5+PPARγ+ transitional basal cells seen in adult follicles (Figure 1F). Furthermore, we observed early sebocytes, identified by the unique co-expression of K79 and PPARγ, located immediately adjacent to the basal layer and alongside K79+ columns (Figure 1F). These findings are consistent with previous studies indicating that basal cells undergo asymmetric cell divisions to form sebocytes,[40,44] and suggest a model for how the SG compartment becomes connected to the developing sebaceous duct and future hair follicle infundibulum, domains that are unified by their shared expression of K79 (Figure 1G). In total, these observations establish a set of landmarks for evaluating SGs.

SG dynamics during skin homeostasis and injury

Given our observation that PPARγ is initially expressed in the SG basal layer, we next attempted to trace the fate of *Pparg*-expressing cells and their progeny. For this, we acquired AdipoTrak mice, in which a tetracycline-regulated transactivator (tTA) is expressed under the control of the endogenous *Pparg* promoter (Figure 2A).[45] When coupled with a tetracycline-responsive element (TRE)-driven Cre recombinase and a Cre-inducible YFP reporter allele (PPARγ;YFP mice), these genetic elements enable PPARγ+ cells and their descendants to become permanently labeled. However, in the presence of doxycycline (doxy), tTA cannot activate Cre expression, providing temporal control over this system.

We began by analyzing 8-week-old PPARγ;YFP mice without doxy exposure (label on), and observed that >98% of all SGs were completely labeled (Figure 2B). These labeled cells included SG basal layer cells, sebocytes, and differentiated cells of the sebaceous duct but did not include the interfollicular epidermis (IFE), isthmus, or other hair follicle compartments. We also did not detect any additional epithelial cell labeling in anagen hair follicles, demonstrating the exquisite specificity for SG labeling in this system (Figure 2B).

To track the long-term fate of labeled cells in the SG, we next treated 8-week-old mice with doxy-containing chow to suppress any additional new labeling (label on → off). After 30 weeks of continuous doxy treatment, we observed that ~86% of SGs were still completely labeled (Figures 2C and 2D). To verify that induction of YFP labeling is indeed suppressed by doxy-chow, we examined adult mice that were continuously treated with doxy since gestation (label off) and observed no SG labeling, as expected (Figure 2C). These findings suggest that, under homeostatic conditions, SGs are largely self-maintained by their own dedicated stem cell pools but may receive occasional cellular input from the hair follicle.

Following skin injury, stem cells from the IFE and hair follicle migrate into the wound to promote re-epithelialization.[24,46–49] To determine whether SG-derived cells exhibit similar behavior, we generated mice with labeled SGs, treated them with doxy to suppress any additional labeling (label on → off), and subsequently performed excisional wounding. One week after injury, we observed labeled cells that had moved directly out of the SG and into the migratory epithelial front (Figure 2E). These SG-derived cells contributed long term to the regenerated epidermis, since labeled cell clones were still observed at least 8 weeks after wounding (Figure 2E). Notably, after skin healing, we observed that only ~10% of SGs located closest to the wound remained labeled, whereas nearly all SGs situated away from the wound were YFP+ (Figures 2F and 2G). This

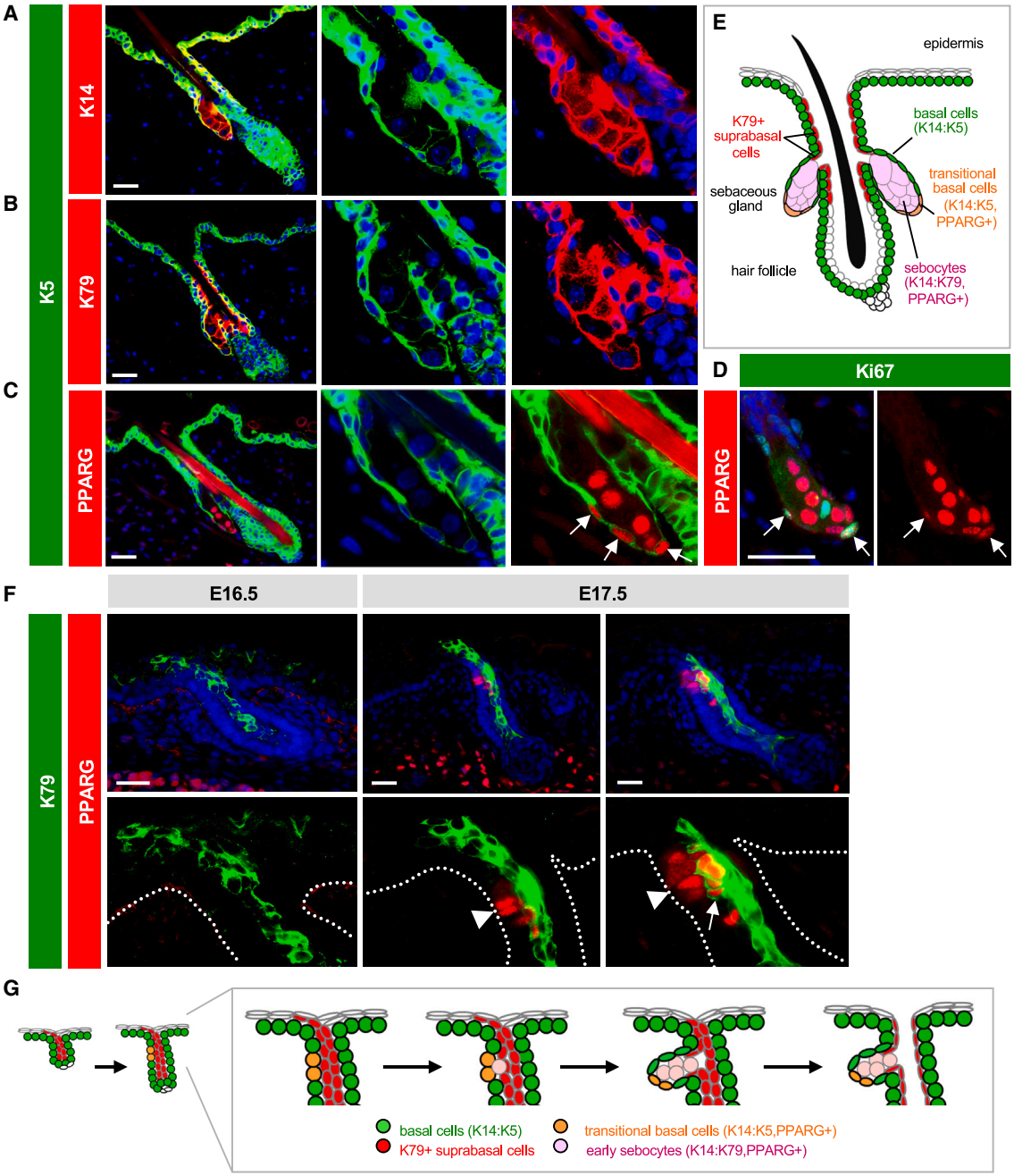

Figure 1. Establishing SG landmarks

(A) Co-localization of K5 (green) with K14 (red) in peripheral SG basal cells, but not in sebocytes. Middle and right panels are magnified single-channel views.

(B) Lack of co-localization of K5 with K79 (red) in sebocytes.

(C) Co-localization of K5 with PPARγ (red) in transitional basal cells of the lower SG (arrows).

(D) Co-localization of PPARγ (red) with Ki67 (green) in a subset of peripheral basal cells (arrows) in the SG.

(E) Schematic of telogen hair follicle. Note that the infundibulum and sebaceous ducts are continuously lined by differentiated K79+ cells (red).

(F) Localization of K79 (green) and PPARγ (red) in the developing hair follicle during embryonic (E) days 16.5–17.5. Middle panels, follicle with basal PPARγ+ cells (arrowhead), but minimal co-localization with K79. Right panels, follicle with early sebocytes identified by the unique co-localization of PPARγ and K79 (arrow). Dotted lines delineate the basal layer of the epidermis and hair follicle. Bottom panels are magnified views, with DAPI omitted for clarity.

(G) Schematic of SG specification. PPARγ+ basal cells (orange) initially emerge at E16.5–17.5 and give rise to early sebocytes (pink) adjacent to the K79+ cell column (red). Subsequent remodeling leads to the opening of the sebaceous duct and hair canal.[39] One of two SG lobes is depicted. The second lobe may be specified later or may arise when the initial SG compartment splits into two, as has been proposed.[40] Scale bar, 50 μm.

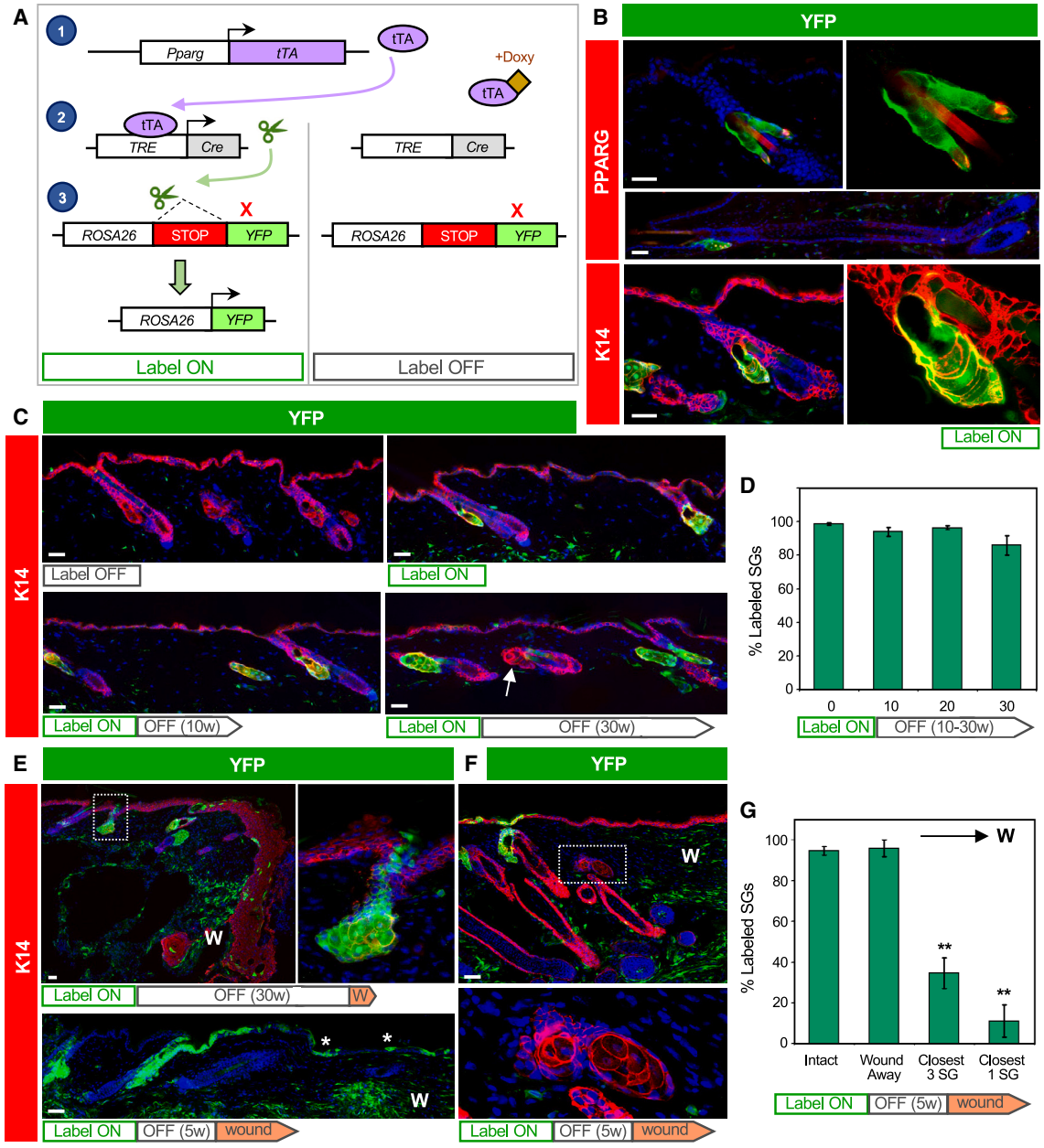

Figure 2. Tracing the SG during homeostasis and after wounding

(A) Schematic for tracing PPARγ+ cells. Left, in the absence of doxycycline (doxy), *Pparg* promoter-driven tTA induces Cre expression, causing genomic recombination that activates YFP expression. Right, doxy suppresses tTA activity.

(B) Immunohistochemical localization of YFP (green) and PPARγ (red, top) or K14 (red, bottom) in label-on PPARγ;YFP mice. Basal SG cells, sebocytes, and sebaceous ducts express YFP, but other hair follicle epithelia do not, in either telogen (top, bottom) or anagen (middle). Right panels are magnified views of the left panels, with DAPI omitted.

(C) Top panels, 8-week-old skin from label-off (left) or label-on (right) PPARγ;YFP mice. Bottom panels, skin from mice treated for the first time with doxy starting at 8 weeks of age, for 10–30 continuous weeks (label-on → label-off). Arrow, unlabeled SG.

(D) Quantitation of labeled SGs, following 0–30 weeks of continuous doxy treatment.

(E) Wounded skin from a label-on → label-off PPARγ;YFP mouse, examined 1 week (top) or 8 weeks (bottom) after injury. Top right panel is a magnified view of the boxed area showing labeled cells that have departed the SG and entered the epidermis. Asterisk, SG-derived YFP+ cells maintained long-term in the healed epithelium. K14 staining was omitted from the bottom panel for clarity.

(legend continued on next page)

suggests that injury can spur a dramatic reorganization of the SG, where resident SG progenitors depart their niche and are replaced by unlabeled hair follicle-derived stem cells. The absence of labeling in wound-proximal SGs also provides technical reassurance that *de novo* labeling of SGs is properly suppressed by doxy treatment.

Sebocyte isolation

Having characterized the cell dynamics of SGs during homeostasis and injury, we next sought to investigate the molecular changes that occur during sebocyte differentiation. While previous scRNA-seq studies on mouse and human skin have included SG sub-populations, these cells are poorly represented due to challenges associated with isolating large, complex, lipid-filled sebocytes. Since PPARγ;YFP mice exhibit specific labeling of SGs, we analyzed skin epithelial cell suspensions by flow cytometry and found that YFP+ cells typically comprise 2%–4% of live cells recovered from 8-week-old label-on mice (Figure 3A). By further fractionating YFP+ cells by size and complexity (measured by forward scatter [FSC] and back scatter [BSC]), followed by staining plated cells with the lipophilic dye Nile red, we observed that the vast majority of Nile red+ sebocytes are found within the highest ∼10% FSC/BSC sub-population (Figures 3A and 3B). In contrast, FSC/BSC-low YFP+ cells were only occasionally stained by Nile red and likely comprise a mix of smaller SG basal progenitors, early sebocytes, and sebaceous duct cells (Figure 3B). Overall, this approach enabled us to significantly enrich for SG cells and especially sebocytes, which accounted for <1% of all cells in our original suspension.

Characterizing initial sebocyte differentiation

After devising a strategy to isolate SG cells, we performed targeted scRNA-seq on YFP+ cells sorted from 8-week-old skin and visualized these data in two-dimensional space by Uniform Manifold Approximation and Projection (UMAP) using Seurat. We identified seven cell clusters, including three sebocyte clusters (SEB1–3) that exhibit expression of established SG biomarkers (*Pparg*, *Scd1*, *Fasn*, *Cidea*) (Figures 3C and 3D). We also identified one cluster representing SG basal cells (BAS) that expresses high level *Krt5*, *Krt14*, and *Lrig1*, which encode markers of SG stem cells[24] (Figures 3C, 3E, and 3F). Flanking the BAS cluster, one minor cluster likely comprises mixed upper hair follicle (uHF) cells of the infundibulum and sebaceous duct, as assessed by markers *Krt79*, *Krt17*, *Krt10*, *Cst6*, *Plet1*, *Defb6*, and *Gata6*, cataloged previously by us and others (Figures 3C, 3E, 3F, S1A, and S1B).[43,50–53] A second minor cluster consists of blended *Krt5*+ basal and *Krt1*+ suprabasal cells of the IFE, likely originating from SG cells that had departed their niche following mild skin agitation such as scratching (Figures 3C and S1A).

Notably, a final cell cluster extended out from the BAS cluster toward the SEB sub-populations. Cells in this cluster uniquely express a combination of basal markers (*Krt14*, *Krt5*) as well as sebocyte differentiation markers (*Pparg*), strongly suggesting that these are the K5+PPARγ+ transitional basal cells (t-BAS) identified above (Figures 1C, 3C, and 3G). Also consistent with our above findings, we observed that downstream of the t-BAS state, all differentiated SEB clusters express *Krt14* and *Krt79*—but not *Krt5*—reinforcing the notion that SG progenitors undergo a K14:K5 → K14:K79 keratin shift during sebocyte differentiation (Figure 3G). Indeed, aside from *Krt14* and *Krt79*, no other keratins were expressed at appreciable levels in the 3 SEB clusters (Figure S1A), consistent with our previous observation that K79 serves a non-redundant structural role in the SG.[20]

To infer cell-state transitions between clusters, we next performed RNA-velocity analysis using scVelo and visualized trajectories using partition-based graph abstraction (PAGA). A steady-state model of transcriptional dynamics predicted a trajectory whereby BAS cells pass through the t-BAS transitional state to become SEB1 cells (Figure 3H, left). However, a dynamic model also predicted that a subset of BAS cells can bypass the t-BAS state to directly become SEB1 cells (Figure 3H, right). Overall, our findings suggest that, during homeostasis, resident SG basal progenitors can take either an indirect or direct path to differentiate into SEB1 sebocytes (Figure 3I).

Characterizing sebocyte cell states

Once specified, sebocytes accumulate lipids and undergo a specialized degradative process to release sebum. To better understand the cell-state transitions that occur during sebocyte maturation, we visualized the pseudotemporal dynamics of SG cells using Monocle 2, which ordered the cells in a linear trajectory without significant branching. Although the minor uHF and IFE cell states were inter-mixed by this analysis, a single trajectory pointed from BAS to t-BAS, and then sequentially through SEB-1, -2, and -3 terminal states, consistent with results by RNA-velocity analysis (Figures 4A and 4B).

We next identified pseudotime-dependent differentially expressed genes (DEGs) and performed Gene Ontology (GO) analysis to identify cellular processes that become altered during sebocyte maturation. Across the pseudotime trajectory, 3,753 DEGs were identified and grouped by K-medoid clustering into six gene modules with distinct expression patterns and biological functions. Notably, three modules (C1, C5, C4) of gene expression changes were increased in sebocytes relative to the other cell populations. These modules included genes associated with lipid metabolism, endoplasmic reticulum (ER) stress response, autophagy, and aerobic respiration (Figure 4C). By contrast, three modules (C2, C3, C6) were decreased in sebocytes and were associated with cell functions such as mRNA processing, translation, chromatin organization, and cytoskeletal processes (Figure 4D). Finally, expression of androgen receptor and androgen response genes was increased during sebocyte differentiation (Figures S1B and S1C).[8,37,54,55] Taken together,

(F) Wounded skin from a label-on → label-off PPARγ;YFP mouse, examined 3 weeks after injury. Bottom panel is a magnified view of the boxed area showing unlabeled, wound-proximal SGs.

(G) Quantitation of SG labeling as a function of distance from the wound site. The closest SG cluster to the wound site is designated "closest 1," and the closest 3 SG clusters are designated "closest 3." W, wound site. w, weeks. **$p < 0.01$ by one-way ANOVA and Tukey *post hoc* test, comparing closest 3 or closest 1 with "intact" or "wound away." $n \geq 4$ mice per time point for (D). Four mice were wounded for (G). Data are represented as mean ± SEM. Scale bar, 50 μm.

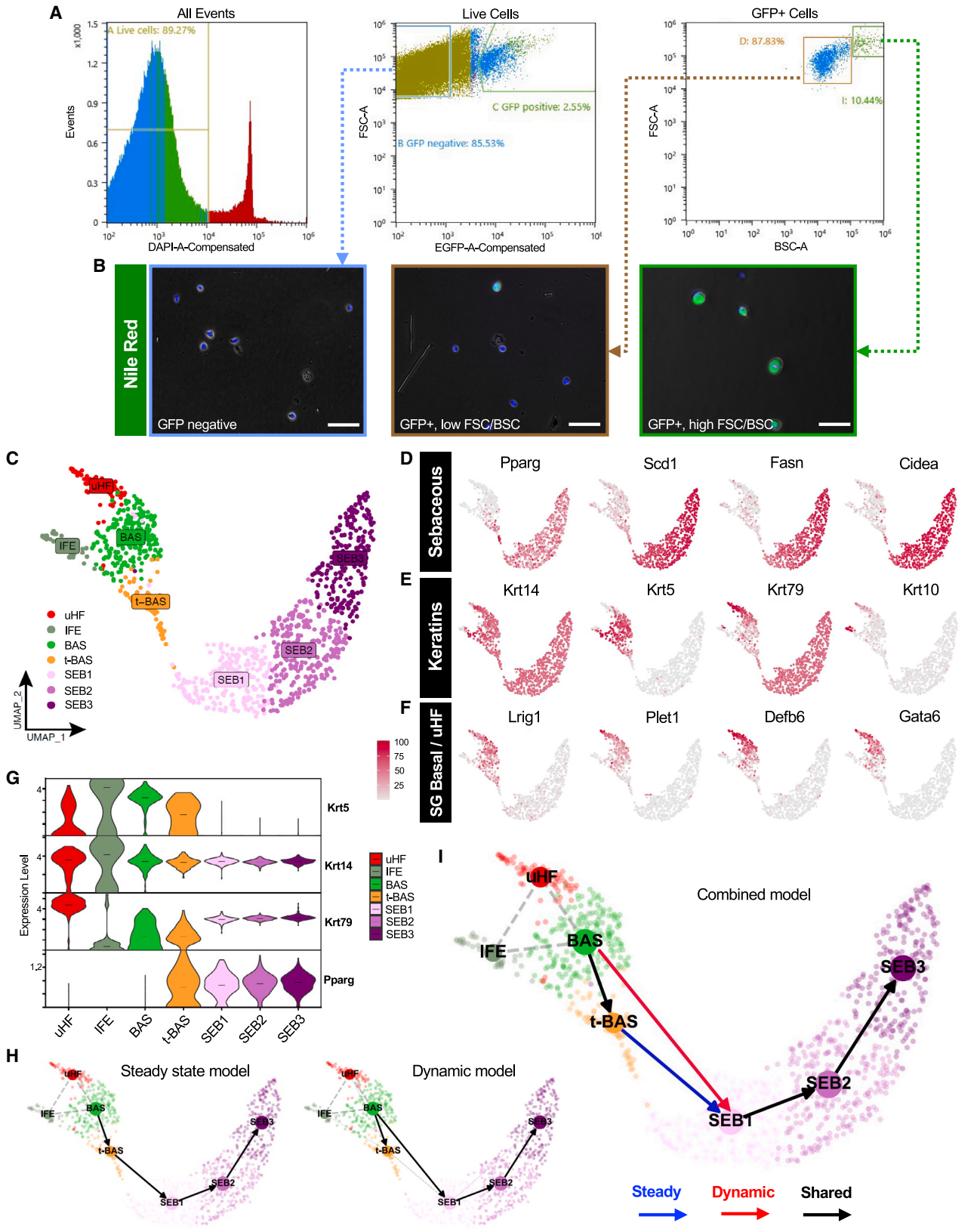

(legend on next page)

these changes indicate that sebocytes comprise a terminally differentiating, hormone-responsive cell lineage characterized by the shutdown of core cellular processes, the degradation of key structural components, and finally autophagic cell death.

Spatially mapping sebocyte cell states

Our RNA-velocity and pseudotime analyses both suggest that sebocytes undertake a unidirectional SEB-1 → SEB-2 → SEB-3 trajectory. This path is further supported by a stepwise elevation in expression of canonical SG markers, such as *Scd1*, *Fasn*, and *Mc5r* (Figure 5A). To spatially resolve the three SEB clusters in the SG, we identified DEGs that define each cell state and found that SEB-1 cells are enriched for *Acp5* and *Mgst2* expression (Figures 5A and S2). Although the SEB-2 cluster appears to represent an intermediate state with no unique markers, SEB-3 cells display increased *Awat1* and *Slc6a19* mRNA (Figures 5A and S2).

By RNAscope *in situ* staining, we next confirmed that expression of *Acp5* and *Mgst2* (SEB-1) is predominantly localized to the lower SG (Figure 5B). On the other hand, expression of *Awat1* and *Slc6a19* (SEB-3) is enriched in sebocytes occupying a more central position in the gland (Figure 5B). For all four genes, we further observed that their expression patterns are recapitulated in skin treated with calcipotriol (MC903), a vitamin D analog that causes SG enlargement, facilitating the visualization of lower-abundance transcripts (*Mgst2*, *Slc6a19*) (Figure 5B).

Finally, we observed an additional sebocyte population that is rarely stained by any RNAscope probes, including probes targeted against pan-sebocyte markers such as *Pparg* and *Krt79* (Figures 5A and 5C). These sebocytes, located at the distal end of the gland, closest to the sebaceous duct, comprise roughly 20%–50% of the total SG volume, and likely represent the most terminal cell state downstream of SEB-3. Because these terminal sebocytes are RNA-low, they are likely not represented in our scRNA-seq dataset. Overall, our findings suggest that resident basal progenitors differentiate into SEB1 sebocytes primarily in the lower SG and that these sebocytes transition unidirectionally along multiple cell states as they move toward the sebaceous duct, as summarized in Figure 5D.

SGs regenerate following genetic ablation

Given that *Pparg* is expressed in both the t-BAS and SEB1-3 cell states (Figure 5A), we next tested its requirement for SG homeostasis in adult skin. We therefore generated mice expressing tamoxifen-inducible Lrig1-CreERT2 coupled with homozygous conditional alleles for *Pparg* (LP mice), which enables targeted deletion of *Pparg* in SG stem cells.[56,57] When 8-week-old LP mice were treated with tamoxifen (TAM)-containing chow for five continuous weeks, 99% of SGs were ablated from dorsal skin, confirming the absolute requirement for PPARγ in SG maintenance (Figure 6A).[58] Surprisingly, however, when these LP mice were subsequently removed from TAM treatment ("chase"), roughly half of all SGs reappeared within 5 weeks, with full recovery seen after 15 weeks' chase (Figures 6A and 6B). Regenerated SGs expressed PPARγ, indicating that they were derived from cells that had not undergone Cre-mediated recombination (Figure S3A). Since SG regeneration has not been previously documented, these observations propelled our studies in an unexpected direction.

Cellular mechanisms for SG regeneration

To better understand how SGs regenerate, we checked whether PPARγ is fully ablated from the hair follicle. In LP mice treated with TAM-chow for 5 weeks (no chase), we observed that PPARγ is almost completely abolished from the isthmus/junctional zone, as expected, leaving behind residual "nubs" of K5+PPARγ-negative cells (Figures 6C and S3B). However, we also occasionally observed very faint PPARγ staining, at an intensity level far lower than what is seen in skin when only one copy of *Pparg* is intentionally deleted (*Pparg-flox*/+, or LP-Het) (Figure 6C). Thus, trace PPARγ staining in LP follicles is unlikely to be caused by incomplete recombination within the Lrig1+ domain. Rather, this may reflect cells that had newly entered the isthmus and had either recently begun expressing PPARγ or had recently deleted PPARγ. Faint PPARγ staining was seen even in LP mice that were treated with TAM-chow for 10 continuous weeks (not shown), and here again PPARγ+ SGs regenerated with similar kinetics after TAM removal (Figures 6D and 6E).

If non-recombined cells enter the isthmus following SG ablation, where are they coming from? To address this, we examined LP mice at earlier time points after ceasing TAM treatment. Interestingly, in LP mice treated with TAM-chow for 5 weeks, followed by a shorter 2 weeks' chase, we observed ectopic PPARγ expression in basal cells within the upper outer root sheath of anagen follicles (Figures 6F and S3C). This domain has previously been shown to be derived from bulge cells,[59] which we

Figure 3. Isolating and profiling SG cells

(A) Flow cytometry plots of isolated cell suspensions from 8-week-old PPARγ;YFP label-on skin.

(B) Nile red staining (green) of sorted keratinocyte sub-populations: bulk GFP negative (left), GFP+ with low FSC/BSC (middle), and GFP+ with high FSC/BSC (right). Note that GFP epifluorescence is not visible and does not interfere with bright Nile red staining, which was superimposed upon bright-field images.

(C) UMAP projection showing seven cell clusters isolated from YFP-sorted, 8-week-old PPARγ;YFP label-on skin.

(D) Feature plots for canonical SG genes.

(E) Feature plots for key keratin genes.

(F) Feature plots for markers of SG basal cells, sebaceous duct, isthmus, and infundibulum.

(G) Violin plots showing relative expression of key marker genes across different cell sub-populations. Note that t-BAS cells uniquely express both *Krt5* and *Pparg*. Horizontal lines indicate median values.

(H) RNA-velocity trajectory analysis performed using scVelo with either a steady-state (left) or dynamic (right) model.

(I) Trajectory analysis incorporating results from both steady-state and dynamic models, suggesting that BAS cells enter the transitional t-BAS state before differentiating into SEB-1 sebocytes (blue arrow) or can differentiate directly into SEB-1 sebocytes (red arrow). Black arrows, lineage relationships identified by both models. Gray dotted lines indicate statistical connectivity between clusters. Trajectories predicted by scVelo originating from the IFE were removed for clarity. Scale bar, 50 μm. See also Figures S1 and S2, Data S1 and S2.

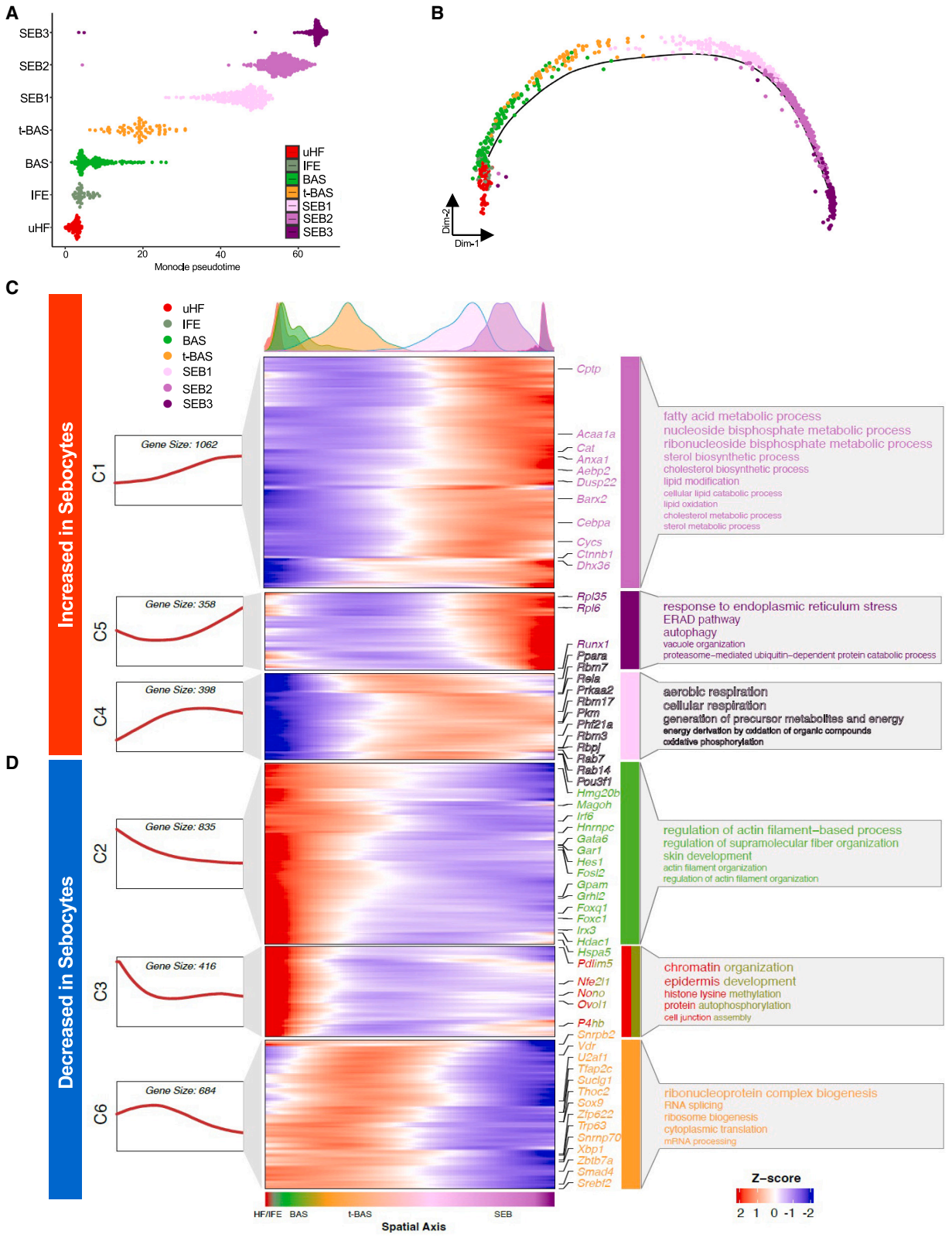

Figure 4. Pseudotemporal dynamics of gene expression during sebocyte differentiation

(A and B) Pseudotemporal ordering of seven cell sub-populations isolated from YFP-sorted, PPARγ;YFP label-on skin using Monocle 2.

(legend continued on next page)

confirmed are not targeted by Lrig1-CreERT2 (Figure S3D). In addition, we observed high-level PPARγ expression reappearing in basal cells at the isthmus, which can also be derived from upper bulge cells over time (Figure 6F).[60] Altogether, our findings suggest that non-recombined bulge-derived cells rapidly migrate into the isthmus/junctional zone to regenerate SGs following genetic ablation. In contrast to homeostatic self-renewal, this regenerative process is likely akin to the recruitment of replacement SG progenitors after skin wounding (Figures 2E and 2F).

Modulation of SG regeneration by hair cycle and fibroblast growth factor signaling

As a final question, we asked what signals instruct progenitor cells to regenerate SGs. For this, we shortened the experimental window and treated 6-week-old LP mice with TAM-chow for 2 weeks (no chase), which caused a 97% reduction in PPARγ+/Scd1+ SGs (Figures 7A and S3E). At this point, hair follicles have uniformly entered the telogen resting phase at 8 weeks of age. Since subsequent re-entry to anagen growth is asynchronous in adult skin, this provided us the opportunity to assess SG regeneration in anagen and telogen skin from the same animal (Figures 7B and 7C). Indeed, we observed that, 5 weeks after TAM withdrawal, anagen skin exhibited a >6-fold increase in SGs compared to adjacent telogen skin from the same animal (Figure 7C).

To better explore the connection between hair growth and SG regeneration, we next depilated 8-week-old LP mice immediately after completing a 2-week course of TAM treatment. Depilation-induced anagen skin similarly exhibited a >10-fold increase in PPARγ+/Scd1+ SGs compared to non-depilated skin from the same animal (Figures 7D and 7E). These effects were quantitated 2 weeks after depilation/TAM removal, but differences in SG regeneration were apparent even after just 10 days, when most follicles in depilated skin were in early anagen (Figure 7F).

Lastly, to identify factors that modulate SG regeneration, we turned back to our scRNA-seq data and found that *Fgfbp3*, which encodes a potentiator of fibroblast growth factor (FGF) signaling,[61] is among only a handful of genes for secreted factors whose expression is enriched in the SEB lineage (Figure S4A). Furthermore, we noted that, among the four major FGF receptors (FGFRs) in mice, only *Fgfr2* is expressed in the SG (Figures S4A and S4B), consistent with enriched FGFR2 localization seen in SG basal and transitional basal layer cells (Figure S4C). We therefore treated LP mice with the FGFR2 inhibitor pemigatinib (pemi)[62] and examined SG regeneration after depilation. Although FGFR2 inhibition did not prevent hair follicles from re-entering anagen (Figure S4D), significantly fewer SGs regenerated in pemi-treated mice compared to vehicle-treated controls (Figures 7G, 7H, and S4E). This effect was associated with fewer phosphorylated-p44/42 (pErk1/2) mature sebocytes in pemi-treated mice, while overall levels of FGFR2 appeared unchanged (Figures S4C, S4F, and S4G). Altogether, these findings identify a robust and previously unrecognized process for regenerating SGs that can be modulated by hair growth and FGFR2 signaling.

DISCUSSION

Numerous technical challenges have long hindered the study of SGs. In particular, Cre-mediated approaches for manipulating these appendages typically drive genetic recombination in multiple skin compartments, complicating the interpretation of results. Although mice expressing a sebocyte-specific, *Scd3* promoter-driven Cre have been reported, this system likely does not cause recombination in SG basal layer cells, and recombination efficiency in sebocytes remains unclear.[63] Another long-standing challenge has been the inability to purify SG cells for molecular profiling. Indeed, we observed that sebocytes constituted <1% of all cells prior to enrichment, consistent with their relative paucity in published scRNA-seq atlases of mouse and human skin.[26–28]

By overcoming multiple technical hurdles, our study paints a vibrant portrait of the cellular and molecular architecture of SGs during development, homeostasis, wounding, and regeneration. Several themes have emerged. First, SGs are largely self-renewed by resident stem cell pools during homeostasis, although cells originating from outside the gland can also occasionally contribute. Second, when the SG stem cell niche is perturbed, either by wounding or genetic ablation, alternative stem cells rapidly enter the SG domain to repopulate the gland. These findings are consistent with the view that stem cells within discrete hair follicle niches serve largely compartmentalized roles during homeostasis but become highly plastic following injury.[19,48,64]

A third theme is that, while PPARγ is essential for sebocyte differentiation, this transcription factor is initially expressed in SG basal cells. This is seen during development, homeostasis, and regeneration. We should emphasize that these t-BAS transitional basal cells—which represent the earliest cells in the SG to express *Pparg* but also the latest cells to express high-level *Krt5* (Figures 1C and 3G)—are unlikely to be SG stem cells in adult skin. Similar to transitional basal cells in the IFE that express differentiation markers such as K10, these K5+PPARγ+ cells likely possess limited replication potential and are poised to differentiate.[65–68] While we cannot formally rule out the possibility that t-BAS cells can revert back to PPARγ-negative basal (BAS) cells, which are likely the stem cells that maintain the SG during homeostasis, such a path is not supported by our scRNA-seq trajectory analysis (Figure 3I).

If expression of PPARγ indeed predisposes basal cells to differentiate into sebocytes, this raises the question of how the entire SG, including PPARγ-negative basal cells, becomes

(C and D) Rolling-wave plot and smoothed expression pattern of pseudotime-dependent genes (n = 3,753) that cluster into six gene modules (C1–C6). Peak positions of the cell populations were visualized by kernel density estimation (top), along the pseudospatial axis (bottom). Also shown are the corresponding expression curve (left) and representative enriched GO terms (right) for each gene module, with larger font size corresponding to increased statistical significance. Transcription factors from each module are indicated. See also Data S3 and S4.

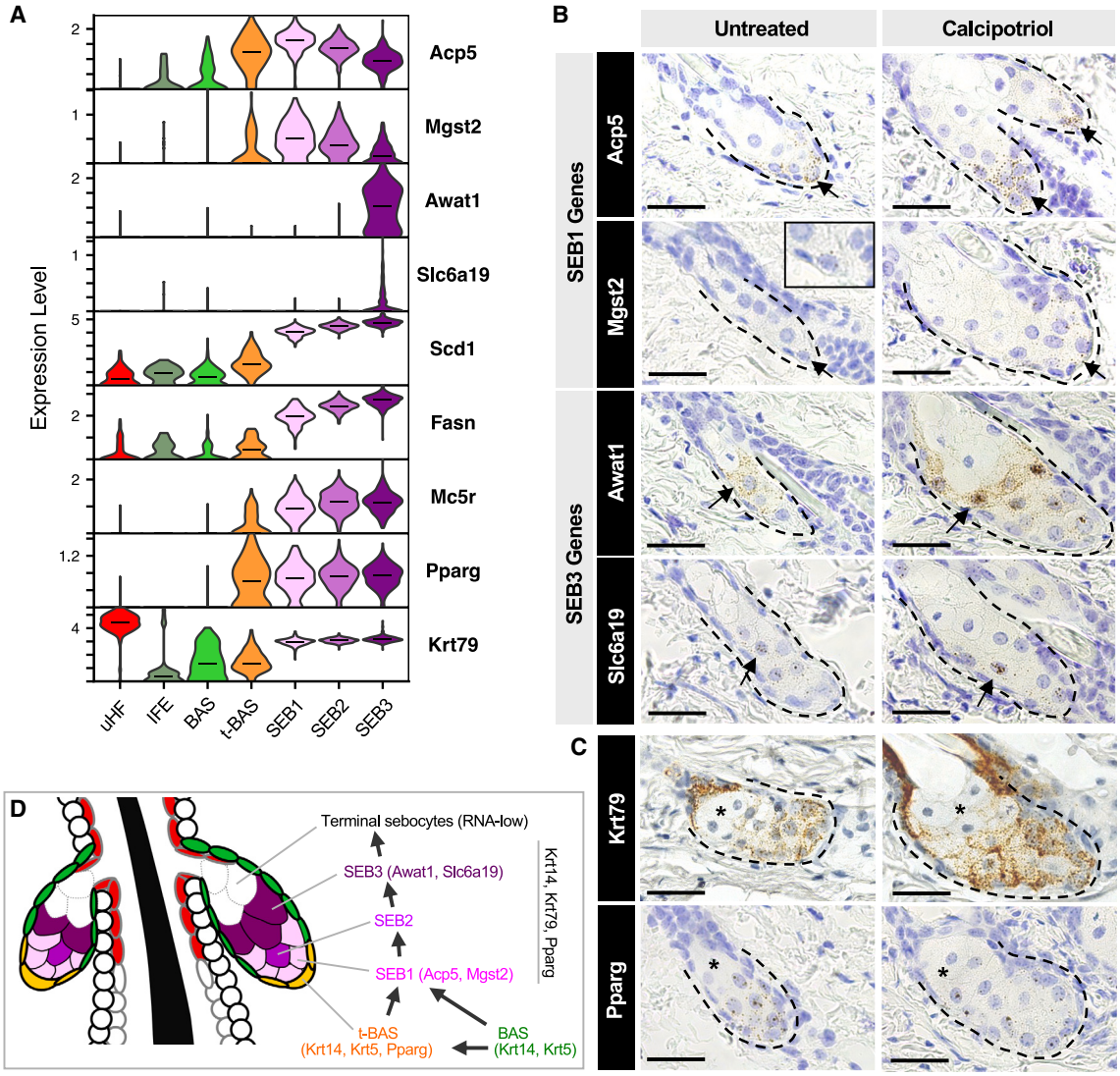

Figure 5. Spatial mapping of different sebocyte cell states

(A) Violin plots showing relative expression of key marker genes in the SG. Horizontal lines indicate median values.

(B) RNAscope *in situ* staining for genes enriched in SEB-1 (*Acp5*, *Mgst2*), and genes enriched in SEB-3 (*Awat1*, *Slc6a19*). Arrow, region where gene is highly expressed. Inset, magnified view of *Mgst2* staining.

(C) RNAscope staining for *Krt79* and *Pparg* in the SG. Asterisk, RNA-low terminal sebocytes. Left column, untreated wild-type skin. Right column, calcipotriol-treated skin.

(D) Schematic summarizing both direct and indirect paths for differentiation of SG basal cells into sebocytes. Scale bar, 50 μm.

labeled in adult PPARγ;YFP label-on mice. Unfortunately, examining newborn skin provided little clarity, as early labeling can be seen in both PPARγ+ and PPARγ-negative cells dispersed around the developing upper follicle prior to formation of the mature SG (Figure S5A). Additional studies are needed to clarify how these patterns resolve over time to achieve specific labeling of the entire adult SG. Related to this, we were also unable to acutely switch on labeling of PPARγ+ cells in adult mice that were maintained on doxy-containing chow and subsequently moved onto normal chow (label off → on) (Figure S5B). The reason for this remains unclear; nonetheless, this technical limitation prevented us from tracing the fate of adult PPARγ+ cells.

Previous studies using multi-color lineage tracing have reported that basal cells located along the entire SG periphery can give rise to differentiated sebocytes.[21] While our trajectory analyses suggest that BAS progenitors can directly form sebocytes without transitioning through the t-BAS intermediate state, both the direct and indirect paths for sebocyte formation invariably funnel through the SEB-1 state, before moving unidirectionally along progressively more differentiated SEB-2 and SEB-3 lineages. A final, terminal cell state—defined not by scRNA-seq but instead by low-level RNA *in situ* staining—juxtaposes the sebaceous duct (Figures 5B and 5C). Since SEB-1 sebocytes are located near the proximal end of the SG, this implies that new

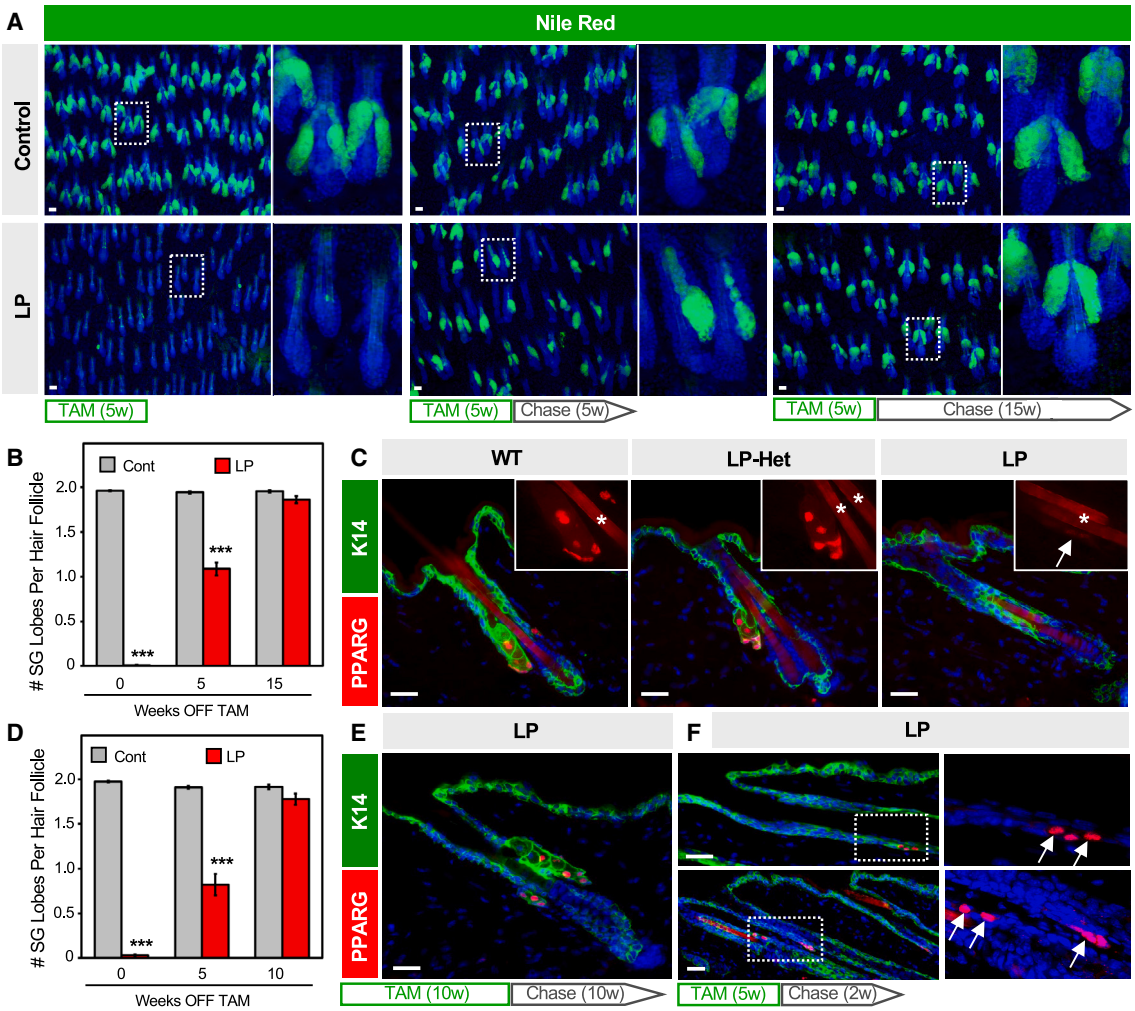

Figure 6. SGs regenerate following genetic ablation

(A) Nile red staining (green) of skin whole mounts from control or LP mice treated with tamoxifen (TAM)-containing chow for five continuous weeks, then moved onto normal chow ("chase") for an additional 0 (left), 5 (middle), or 15 (right) weeks. Right panels are magnified views of the boxed areas.

(B) Quantitation for (A).

(C) Localization of PPARγ (red) in wild-type (left), *Lrig1-CreERT2;Pparg-flox*/+ (LP-Het, middle) or LP mice (right) following 5 weeks of TAM-chow. Insets, magnified views of PPARγ staining. Arrow, faint PPARγ staining at the hair follicle isthmus in LP skin. Asterisk, hair shaft autofluorescence.

(D) Quantitation of SGs similar to (B) but for mice treated with 10 continuous weeks of TAM-chow, followed by 0–10 weeks' chase.

(E) Regenerated SGs express PPARγ (red).

(F) Expression of PPARγ (red, arrows) in basal K14+ cells (green) of the upper anagen ORS (top panels) and isthmus (bottom panels), after 5 weeks of TAM-chow and 2 weeks' chase. Right panels are magnified single-channel views of the boxed areas. w, weeks. ***$p < 0.001$ by unpaired t test comparing control (cont) and LP skin from the same time point. $n \geq 7$ mice, per genotype, per time point for (B) and (D). Data are represented as mean ± SEM. Scale bar, 50 μm. See also Figure S3.

sebocyte formation also primarily occurs within the lower SG. Why our observations differ from those of previous reports remains unclear, but it may have to do with the complex geometry of the gland, as well as differences in experimental timing.

Unexpectedly, we observed that SGs regenerate following genetic ablation of PPARγ and that non-recombined, bulge-derived cells likely give rise to regenerated glands. Although we detected ectopic PPARγ expression in the upper outer root sheath (ORS) of mutant follicles (Figure 6F), SGs reappeared at the original sites from where they were lost. These findings demonstrate that bulge-derived cells—which can either move upward after wounding or downward during hair growth—have the potential to express PPARγ upon departing their niche. At the same time, the factors that specify the exact site of SG development and regeneration remain elusive. Some of these factors likely involve gradients of Wnt and Hedgehog signaling, as well as AP-1 transcription factor activity, since perturbation of any of these components can drive ectopic SG formation.[18,69–71] These gradients may potentially specify both permissive sites for SG formation, as well as non-permissive zones, such as the ORS, which does not form SGs in spite of ectopic PPARγ expression in LP mutants.

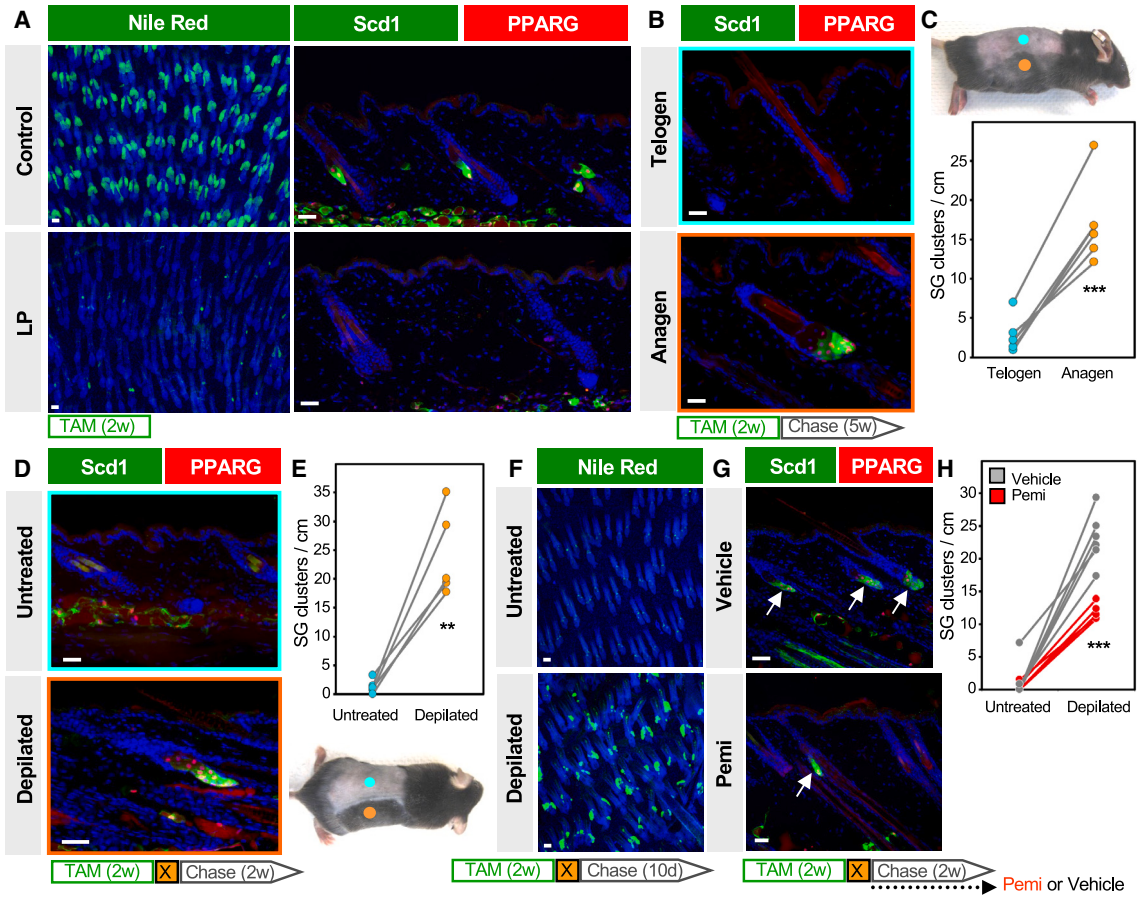

Figure 7. SG regeneration is modulated by hair cycling and FGFR signaling

(A) Left, Nile red (green) staining of skin whole mounts from control (top) or LP (bottom) mice treated with TAM-chow for two continuous weeks (no chase). Right, confirmation of SG loss by staining for Scd1 (green) and PPARγ (red).

(B) Scd1/PPARγ staining in telogen (top) or anagen (bottom) skin from the same animal, following 2 weeks of TAM-chow and 5 weeks' chase.

(C) Top, example of LP mouse treated with TAM-chow for 2 weeks, followed by 5 weeks' chase. Sites of natural anagen (orange) or telogen (blue) are denoted. Bottom, SG quantitation for (B). Paired samples are connected by lines.

(D) Identification of regenerated SGs by Scd1/PPARγ staining in mice treated with TAM-chow for two continuous weeks, then depilated (X) and chased for two additional weeks.

(E) Bottom, example of LP mouse used in (D). Sites of depilation (orange) or no treatment (blue) are denoted. Top, quantitation of SG abundance for (D). Paired samples are connected by lines.

(F). Nile red (green) staining of whole mounts from untreated (top) or depilated (bottom) LP skin, where mice were treated with TAM-chow for 2 weeks, depilated, and chased for 10 days.

(G) Identification of regenerated SGs by Scd1/PPARγ staining (arrows), with similar treatment protocol as in (D) but with additional daily treatment with FGFR inhibitor (pemi) or vehicle during the 2-week chase period.

(H) Quantitation for (G) in LP mice treated with vehicle (gray) or pemi (red). Samples from the same mouse are connected by lines. w, weeks; d, days. $^{**}p < 0.01$, $^{***}p < 0.001$. Paired t test for (C) and (E); unpaired t test comparing only depilated samples for (H). n = 6 mice for (C), n = 5 mice for (E), and n = 11 mice for (H). Scale bar, 50 μm. See also Figures S4 and S5.

Our hair cycle studies also revealed that anagen hair growth, a process associated with increased cell proliferation and movement, greatly accelerates SG regeneration.[19] In contrast, SGs hardly regenerate in telogen skin, indicating that follicles do not automatically regenerate SGs by default. Rather, microenvironmental factors in the skin are likely also critical. At least one of these factors may be Fgfbp3, which binds and liberates FGFs from the extracellular matrix to activate FGFRs.[61] Although *Fgfbp3* null mice do not possess obvious skin defects,[72] mutant mice lacking FGFR2 have smaller SGs in tail skin.[73] Concordantly, acute genetic deletion of *Fgfr2* causes atrophy of eyelid meibomian glands, which are highly related to SGs, and these glands can also partially recover over time.[74,75] Other glandular epithelia, such as mammary and prostate glands, can similarly regenerate after experimental injury in a manner that recapitulates embryonic development.[76]

While SG regeneration has not been previously reported, SG loss or hypoplasia has been associated with several skin pathologies, including cicatricial alopecia, psoriasis, and atopic dermatitis.[4,33,34,36] Chemotherapy can also induce SG

atrophy,[77] while lymphocytic attack of SGs has been observed in a mouse model of acute graft-versus-host disease.[78] Isotretinoin, which is used to treat severe acne, reduces SG size by up to 90%.[79,80] Even in normal skin, SG size and activity increase and diminish at different stages throughout life.[11,81] Whether SGs undergo regeneration in these varied contexts remains unclear but is conceivable in light of our findings. In summary, our work identifies distinct mechanisms for SG maintenance and regeneration, which may ultimately enable these appendages to be preserved following challenges to the skin.

Limitations of the study

Because PPARγ+ t-BAS cells are unlikely to be stem cells, it remains unclear why the entire SG, including PPARγ-negative BAS cells, are labeled in PPARγ;YFP label-on mice. In addition, the direct and indirect pathways for sebocyte differentiation require further characterization, including identifying molecular mediators that govern these cell fate transitions. Similarly, it will be important to clarify the cellular and molecular mechanisms of FGFR2 signaling during SG regeneration and maintenance, especially regarding the identity and source of FGF ligands, which were not expressed by cells in our scRNA-seq dataset. At this time, we cannot formally exclude the possibility that terminal sebocytes appeared low for RNA by *in situ* staining due to artifacts of tissue processing. Finally, future scRNA-seq studies of SGs should incorporate larger cell counts to potentially profile changes in the gland during disease or aging.

STAR★METHODS

Detailed methods are provided in the online version of this paper and include the following:

- KEY RESOURCES TABLE
- RESOURCE AVAILABILITY
  - Lead contact
  - Materials availability
  - Data and code availability
- EXPERIMENTAL MODEL AND STUDY PARTICIPANT DETAILS
  - Animals
- METHOD DETAILS
  - Whole mount analysis
  - Flow cytometry
  - Single cell library preparation
  - Single cell data processing and analysis
  - Immunohistochemistry and RNAscope
- QUANTIFICATION AND STATISTICAL ANALYSIS
  - SG quantitation
  - Statistics

SUPPLEMENTAL INFORMATION

Supplemental information can be found online at https://doi.org/10.1016/j.celrep.2023.113121.

ACKNOWLEDGMENTS

We are grateful to the Dlugosz lab (University of Michigan) for helpful discussions and sharing reagents; Dr. Y. Eugene Chen (University of Michigan) for sharing mice; Ann Marie Deslauriers-Cox for flow cytometry; Dr. Allison C. Billi (University of Michigan) for advice on single-cell preparation; and Tricia Tamsen, Olivia Koues, and the Advanced Genomics Core (University of Michigan) for single-cell sequencing. S.Y.W. acknowledges the support of the LEO Foundation (LF18017) and the NIH (R01AR065409 and R01AR080654). S.X.A. acknowledges the support of the National Science Foundation (CBET2134916). S.Y.W. and S.X.A. were jointly funded by the American Cancer Society (TLC-21-161-01-TLC). S.N. was partly supported by a Japan Society for the Promotion of Science (JSPS) research fellowship. The authors also acknowledge support from the UM Skin Biology and Disease Resource-based Center (P30AR075043) and NCI Cancer Center Support Grant (P30CA046592).

AUTHOR CONTRIBUTIONS

Conceptualization and methodology, N.A.V., Y.Y.J., A.A.D., S.X.A., and S.Y.W.; investigation, N.A.V., A.H., T.J.H., S.Y.T., M.G., S.N., and S.Y.W.; formal analysis, N.A.V., Y.Y.J., S.X.A., and S.Y.W.; writing – original draft, review & editing, N.A.V., Y.Y.J., S.X.A., and S.Y.W.; funding acquisition and supervision, A.A.D., S.X.A., and S.Y.W.

DECLARATION OF INTERESTS

The authors declare no competing interests.

Received: March 24, 2023
Revised: July 1, 2023
Accepted: August 25, 2023

REFERENCES

1. Zouboulis, C.C., Coenye, T., He, L., Kabashima, K., Kobayashi, T., Niemann, C., Nomura, T., Oláh, A., Picardo, M., Quist, S.R., et al. (2022). Sebaceous immunobiology - skin homeostasis, pathophysiology, coordination of innate immunity and inflammatory response and disease associations. Front. Immunol. *13*, 1029818.
2. Niemann, C., and Horsley, V. (2012). Development and homeostasis of the sebaceous gland. Semin. Cell Dev. Biol. *23*, 928–936.
3. Lovászi, M., Szegedi, A., Zouboulis, C.C., and Törőcsik, D. (2017). Sebaceous-immunobiology is orchestrated by sebum lipids. Dermatoendocrinol. *9*, e1375636.
4. Shi, V.Y., Leo, M., Hassoun, L., Chahal, D.S., Maibach, H.I., and Sivamani, R.K. (2015). Role of sebaceous glands in inflammatory dermatoses. J. Am. Acad. Dermatol. *73*, 856–863.
5. Smith, K.R., and Thiboutot, D.M. (2008). Thematic review series: skin lipids. Sebaceous gland lipids: friend or foe? J. Lipid Res. *49*, 271–281.
6. Lee, S.J., Seok, J., Jeong, S.Y., Park, K.Y., Li, K., and Seo, S.J. (2016). Facial Pores: Definition, Causes, and Treatment Options. Dermatol. Surg. *42*, 277–285.
7. Hinde, E., Haslam, I.S., Schneider, M.R., Langan, E.A., Kloepper, J.E., Schramm, C., Zouboulis, C.C., and Paus, R. (2013). A practical guide for the study of human and murine sebaceous glands in situ. Exp. Dermatol. *22*, 631–637.
8. Cottle, D.L., Kretzschmar, K., Schweiger, P.J., Quist, S.R., Gollnick, H.P., Natsuga, K., Aoyagi, S., and Watt, F.M. (2013). c-MYC-induced sebaceous gland differentiation is controlled by an androgen receptor/p53 axis. Cell Rep. *3*, 427–441.
9. Fischer, H., Fumicz, J., Rossiter, H., Napirei, M., Buchberger, M., Tschachler, E., and Eckhart, L. (2017). Holocrine secretion of sebum is a

unique DNase2-dependent mode of programmed cell death. J. Invest. Dermatol. *137*, 587–594.

10. Schneider, M.R., and Paus, R. (2014). Deciphering the functions of the hair follicle infundibulum in skin physiology and disease. Cell Tissue Res. *358*, 697–704.
11. Zouboulis, C.C., and Boschnakow, A. (2001). Chronological ageing and photoageing of the human sebaceous gland. Clin. Exp. Dermatol. *26*, 600–607.
12. Zhang, S., Shui, G., Wang, G., Wang, C., Sun, S., Zouboulis, C.C., Xiao, R., Ye, J., Li, W., and Li, P. (2014). Cidea control of lipid storage and secretion in mouse and human sebaceous glands. Mol. Cell Biol. *34*, 1827–1838.
13. Jung, Y., Tam, J., Ray Jalian, H., Rox Anderson, R., and Evans, C.L. (2015). Longitudinal, 3D in vivo imaging of sebaceous glands by coherent anti-stokes Raman scattering microscopy: normal function and response to cryotherapy. J. Invest. Dermatol. *135*, 39–44.
14. Epstein, E.H., and Epstein, W.L. (1966). New cell formation in human sebaceous glands. J. Invest. Dermatol. *46*, 453–458.
15. Plewig, G., and Christophers, E. (1974). Renewal rate of human sebaceous glands. Acta Derm. Venereol. *54*, 177–182.
16. Weinstein, G.D. (1974). Cell kinetics of human sebaceous glands. J. Invest. Dermatol. *62*, 144–146.
17. Panteleyev, A.A., Rosenbach, T., Paus, R., and Christiano, A.M. (2000). The bulge is the source of cellular renewal in the sebaceous gland of mouse skin. Arch. Dermatol. Res. *292*, 573–576.
18. Petersson, M., Brylka, H., Kraus, A., John, S., Rappl, G., Schettina, P., and Niemann, C. (2011). TCF/Lef1 activity controls establishment of diverse stem and progenitor cell compartments in mouse epidermis. EMBO J. *30*, 3004–3018.
19. Han, J., Lin, K., Choo, H., Chen, Y., Zhang, X., Xu, R.H., Wang, X., and Wu, Y. (2023). Distinct bulge stem cell populations maintain the pilosebaceous unit in a β-catenin-dependent manner. iScience *26*, 105805.
20. Veniaminova, N.A., Grachtchouk, M., Doane, O.J., Peterson, J.K., Quigley, D.A., Lull, M.V., Pyrozhenko, D.V., Nair, R.R., Patrick, M.T., Balmain, A., et al. (2019). Niche-specific factors dynamically regulate sebaceous gland stem cells in the skin. Dev. Cell *51*, 326–340.e4.
21. Andersen, M.S., Hannezo, E., Ulyanchenko, S., Estrach, S., Antoku, Y., Pisano, S., Boonekamp, K.E., Sendrup, S., Maimets, M., Pedersen, M.T., et al. (2019). Tracing the cellular dynamics of sebaceous gland development in normal and perturbed states. Nat. Cell Biol. *21*, 924–932.
22. Füllgrabe, A., Joost, S., Are, A., Jacob, T., Sivan, U., Haegebarth, A., Linnarsson, S., Simons, B.D., Clevers, H., Toftgård, R., and Kasper, M. (2015). Dynamics of Lgr6+ Progenitor Cells in the Hair Follicle, Sebaceous Gland, and Interfollicular Epidermis. Stem Cell Rep. *5*, 843–855.
23. Ghazizadeh, S., and Taichman, L.B. (2001). Multiple classes of stem cells in cutaneous epithelium: a lineage analysis of adult mouse skin. EMBO J. *20*, 1215–1222.
24. Page, M.E., Lombard, P., Ng, F., Göttgens, B., and Jensen, K.B. (2013). The epidermis comprises autonomous compartments maintained by distinct stem cell populations. Cell Stem Cell *13*, 471–482.
25. Kretzschmar, K., Cottle, D.L., Donati, G., Chiang, M.F., Quist, S.R., Gollnick, H.P., Natsuga, K., Lin, K.I., and Watt, F.M. (2014). BLIMP1 is required for postnatal epidermal homeostasis but does not define a sebaceous gland progenitor under steady-state conditions. Stem Cell Rep. *3*, 620–633.
26. Joost, S., Annusver, K., Jacob, T., Sun, X., Dalessandri, T., Sivan, U., Sequeira, I., Sandberg, R., and Kasper, M. (2020). The molecular anatomy of mouse skin during hair growth and rest. Cell Stem Cell *26*, 441–457.e7.
27. Joost, S., Zeisel, A., Jacob, T., Sun, X., La Manno, G., Lönnerberg, P., Linnarsson, S., and Kasper, M. (2016). Single-cell transcriptomics reveals that differentiation and spatial signatures shape epidermal and hair follicle heterogeneity. Cell Syst. *3*, 221–237.e9.
28. Cheng, J.B., Sedgewick, A.J., Finnegan, A.I., Harirchian, P., Lee, J., Kwon, S., Fassett, M.S., Golovato, J., Gray, M., Ghadially, R., et al. (2018). Transcriptional programming of normal and inflamed human epidermis at single-cell resolution. Cell Rep. *25*, 871–883.
29. Zheng, Y., Eilertsen, K.J., Ge, L., Zhang, L., Sundberg, J.P., Prouty, S.M., Stenn, K.S., and Parimoo, S. (1999). Scd1 is expressed in sebaceous glands and is disrupted in the asebia mouse. Nat. Genet. *23*, 268–270.
30. Sundberg, J.P., Boggess, D., Sundberg, B.A., Eilertsen, K., Parimoo, S., Filippi, M., and Stenn, K. (2000). Asebia-2J (Scd1(ab2J)): a new allele and a model for scarring alopecia. Am. J. Pathol. *156*, 2067–2075.
31. Kobayashi, T., Voisin, B., Kim, D.Y., Kennedy, E.A., Jo, J.H., Shih, H.Y., Truong, A., Doebel, T., Sakamoto, K., Cui, C.Y., et al. (2019). Homeostatic Control of Sebaceous Glands by Innate Lymphoid Cells Regulates Commensal Bacteria Equilibrium. Cell *176*, 982–997.e16.
32. Choa, R., Tohyama, J., Wada, S., Meng, H., Hu, J., Okumura, M., May, R.M., Robertson, T.F., Pai, R.A.L., Nace, A., et al. (2021). Thymic stromal lymphopoietin induces adipose loss through sebum hypersecretion. Science *373*, eabd2893.
33. Rittié, L., Tejasvi, T., Harms, P.W., Xing, X., Nair, R.P., Gudjonsson, J.E., Swindell, W.R., and Elder, J.T. (2016). Sebaceous Gland Atrophy in Psoriasis: An Explanation for Psoriatic Alopecia? J. Invest. Dermatol. *136*, 1792–1800.
34. Karnik, P., Tekeste, Z., McCormick, T.S., Gilliam, A.C., Price, V.H., Cooper, K.D., and Mirmirani, P. (2009). Hair follicle stem cell-specific PPARgamma deletion causes scarring alopecia. J. Invest. Dermatol. *129*, 1243–1257.
35. Reichenbach, B., Classon, J., Aida, T., Tanaka, K., Genander, M., and Göritz, C. (2018). Glutamate transporter Slc1a3 mediates inter-niche stem cell activation during skin growth. EMBO J. *37*, e98280.
36. Stenn, K.S., Sundberg, J.P., and Sperling, L.C. (1999). Hair follicle biology, the sebaceous gland, and scarring alopecias. Arch. Dermatol. *135*, 973–974.
37. Zhang, C., Chinnappan, M., Prestwood, C.A., Edwards, M., Artami, M., Thompson, B.M., Eckert, K.M., Vale, G., Zouboulis, C.C., McDonald, J.G., and Harris-Tryon, T.A. (2021). Interleukins 4 and 13 drive lipid abnormalities in skin cells through regulation of sex steroid hormone synthesis. Proc. Natl. Acad. Sci. USA *118*, e2100749118.
38. Pan, X., Hobbs, R.P., and Coulombe, P.A. (2013). The expanding significance of keratin intermediate filaments in normal and diseased epithelia. Curr. Opin. Cell Biol. *25*, 47–56.
39. Mesler, A.L., Benedeck, R.E., and Wong, S.Y. (2021). Preparing the hair follicle canal for hair shaft emergence. Exp. Dermatol. *30*, 472–478. https://doi.org/10.1111/exd.14210.
40. Frances, D., and Niemann, C. (2012). Stem cell dynamics in sebaceous gland morphogenesis in mouse skin. Dev. Biol. *363*, 138–146.
41. Ramot, Y., Mastrofrancesco, A., Camera, E., Desreumaux, P., Paus, R., and Picardo, M. (2015). The role of PPARγ-mediated signalling in skin biology and pathology: new targets and opportunities for clinical dermatology. Exp. Dermatol. *24*, 245–251.
42. Ahmadian, M., Suh, J.M., Hah, N., Liddle, C., Atkins, A.R., Downes, M., and Evans, R.M. (2013). PPARgamma signaling and metabolism: the good, the bad and the future. Nat. Med. *19*, 557–566.
43. Veniaminova, N.A., Vagnozzi, A.N., Kopinke, D., Do, T.T., Murtaugh, L.C., Maillard, I., Dlugosz, A.A., Reiter, J.F., and Wong, S.Y. (2013). Keratin 79 identifies a novel population of migratory epithelial cells that initiates hair canal morphogenesis and regeneration. Development *140*, 4870–4880.
44. Feldman, A., Mukha, D., Maor, I.I., Sedov, E., Koren, E., Yosefzon, Y., Shlomi, T., and Fuchs, Y. (2019). Blimp1+ cells generate functional mouse sebaceous gland organoids in vitro. Nat. Commun. *10*, 2348.
45. Tang, W., Zeve, D., Suh, J.M., Bosnakovski, D., Kyba, M., Hammer, R.E., Tallquist, M.D., and Graff, J.M. (2008). White fat progenitor cells reside in the adipose vasculature. Science *322*, 583–586.
46. Ito, M., Liu, Y., Yang, Z., Nguyen, J., Liang, F., Morris, R.J., and Cotsarelis, G. (2005). Stem cells in the hair follicle bulge contribute to wound repair but not to homeostasis of the epidermis. Nat. Med. *11*, 1351–1354.

47. Vagnozzi, A.N., Reiter, J.F., and Wong, S.Y. (2015). Hair follicle and interfollicular epidermal stem cells make varying contributions to wound regeneration. Cell Cycle *14*, 3408–3417.

48. Huang, S., Kuri, P., Aubert, Y., Brewster, M., Li, N., Farrelly, O., Rice, G., Bae, H., Prouty, S., Dentchev, T., et al. (2021). Lgr6 marks epidermal stem cells with a nerve-dependent role in wound re-epithelialization. Cell Stem Cell *28*, 1582–1596.e6.

49. Haensel, D., Jin, S., Sun, P., Cinco, R., Dragan, M., Nguyen, Q., Cang, Z., Gong, Y., Vu, R., MacLean, A.L., et al. (2020). Defining epidermal basal cell states during skin homeostasis and wound healing using single-cell transcriptomics. Cell Rep. *30*, 3932–3947.e6.

50. Raymond, K., Richter, A., Kreft, M., Frijns, E., Janssen, H., Slijper, M., Praetzel-Wunder, S., Langbein, L., and Sonnenberg, A. (2010). Expression of the orphan protein Plet-1 during trichilemmal differentiation of anagen hair follicles. J. Invest. Dermatol. *130*, 1500–1513.

51. Panteleyev, A.A., Paus, R., Wanner, R., Nürnberg, W., Eichmüller, S., Thiel, R., Zhang, J., Henz, B.M., and Rosenbach, T. (1997). Keratin 17 gene expression during the murine hair cycle. J. Invest. Dermatol. *108*, 324–329.

52. Zeeuwen, P.L.J.M., van Vlijmen-Willems, I.M.J.J., Hendriks, W., Merkx, G.F.M., and Schalkwijk, J. (2002). A null mutation in the cystatin M/E gene of ichq mice causes juvenile lethality and defects in epidermal cornification. Hum. Mol. Genet. *11*, 2867–2875.

53. Donati, G., Rognoni, E., Hiratsuka, T., Liakath-Ali, K., Hoste, E., Kar, G., Kayikci, M., Russell, R., Kretzschmar, K., Mulder, K.W., et al. (2017). Wounding induces dedifferentiation of epidermal Gata6+ cells and acquisition of stem cell properties. Nat. Cell Biol. *19*, 603–613.

54. Bayer-Garner, I.B., Givens, V., and Smoller, B. (1999). Immunohistochemical staining for androgen receptors: a sensitive marker of sebaceous differentiation. Am. J. Dermatopathol. *21*, 426–431.

55. Zouboulis, C.C., Chen, W.C., Thornton, M.J., Qin, K., and Rosenfield, R. (2007). Sexual hormones in human skin. Horm. Metab. Res. *39*, 85–95.

56. Powell, A.E., Wang, Y., Li, Y., Poulin, E.J., Means, A.L., Washington, M.K., Higginbotham, J.N., Juchheim, A., Prasad, N., Levy, S.E., et al. (2012). The pan-ErbB negative regulator Lrig1 is an intestinal stem cell marker that functions as a tumor suppressor. Cell *149*, 146–158.

57. He, W., Barak, Y., Hevener, A., Olson, P., Liao, D., Le, J., Nelson, M., Ong, E., Olefsky, J.M., and Evans, R.M. (2003). Adipose-specific peroxisome proliferator-activated receptor gamma knockout causes insulin resistance in fat and liver but not in muscle. Proc. Natl. Acad. Sci. USA *100*, 15712–15717.

58. Sardella, C., Winkler, C., Quignodon, L., Hardman, J.A., Toffoli, B., Giordano Attianese, G.M.P., Hundt, J.E., Michalik, L., Vinson, C.R., Paus, R., et al. (2018). Delayed hair follicle morphogenesis and hair follicle dystrophy in a lipoatrophy mouse model of Pparg total deletion. J. Invest. Dermatol. *138*, 500–510.

59. Hsu, Y.C., Pasolli, H.A., and Fuchs, E. (2011). Dynamics between stem cells, niche, and progeny in the hair follicle. Cell *144*, 92–105.

60. Brownell, I., Guevara, E., Bai, C.B., Loomis, C.A., and Joyner, A.L. (2011). Nerve-derived sonic hedgehog defines a niche for hair follicle stem cells capable of becoming epidermal stem cells. Cell Stem Cell *8*, 552–565.

61. Taetzsch, T., Brayman, V.L., and Valdez, G. (2018). FGF binding proteins (FGFBPs): Modulators of FGF signaling in the developing, adult, and stressed nervous system. Biochim. Biophys. Acta, Mol. Basis Dis. *1864*, 2983–2991.

62. Liu, P.C.C., Koblish, H., Wu, L., Bowman, K., Diamond, S., DiMatteo, D., Zhang, Y., Hansbury, M., Rupar, M., Wen, X., et al. (2020). INCB054828 (pemigatinib), a potent and selective inhibitor of fibroblast growth factor receptors 1, 2, and 3, displays activity against genetically defined tumor models. PLoS One *15*, e0231877.

63. Dahlhoff, M., Camera, E., Schäfer, M., Emrich, D., Riethmacher, D., Foster, A., Paus, R., and Schneider, M.R. (2016). Sebaceous lipids are essential for water repulsion, protection against UVB-induced apoptosis, and ocular integrity in mice. Development *143*, 1823–1831.

64. Schepeler, T., Page, M.E., and Jensen, K.B. (2014). Heterogeneity and plasticity of epidermal stem cells. Development *141*, 2559–2567.

65. Cockburn, K., Annusver, K., Gonzalez, D.G., Ganesan, S., May, D.P., Mesa, K.R., Kawaguchi, K., Kasper, M., and Greco, V. (2022). Gradual differentiation uncoupled from cell cycle exit generates heterogeneity in the epidermal stem cell layer. Nat. Cell Biol. *24*, 1692–1700. https://doi.org/10.1038/s41556-41022-01021-41558.

66. Cohen, E., Johnson, C., Redmond, C.J., Nair, R.R., and Coulombe, P.A. (2022). Revisiting the significance of keratin expression in complex epithelia. J. Cell Sci. *135*, jcs260594.

67. Aragona, M., Sifrim, A., Malfait, M., Song, Y., Van Herck, J., Dekoninck, S., Gargouri, S., Lapouge, G., Swedlund, B., Dubois, C., et al. (2020). Mechanisms of stretch-mediated skin expansion at single-cell resolution. Nature *584*, 268–273.

68. Wang, S., Drummond, M.L., Guerrero-Juarez, C.F., Tarapore, E., MacLean, A.L., Stabell, A.R., Wu, S.C., Gutierrez, G., That, B.T., Benavente, C.A., et al. (2020). Single cell transcriptomics of human epidermis identifies basal stem cell transition states. Nat. Commun. *11*, 4239.

69. Allen, M., Grachtchouk, M., Sheng, H., Grachtchouk, V., Wang, A., Wei, L., Liu, J., Ramirez, A., Metzger, D., Chambon, P., et al. (2003). Hedgehog signaling regulates sebaceous gland development. Am. J. Pathol. *163*, 2173–2178.

70. Singh, K., Camera, E., Krug, L., Basu, A., Pandey, R.K., Munir, S., Wlaschek, M., Kochanek, S., Schorpp-Kistner, M., Picardo, M., et al. (2018). JunB defines functional and structural integrity of the epidermo-pilosebaceous unit in the skin. Nat. Commun. *9*, 3425.

71. Gu, L.H., and Coulombe, P.A. (2008). Hedgehog signaling, Keratin 6 induction, and sebaceous gland morphogenesis. Am. J. Pathol. *173*, 752–761.

72. Tassi, E., Garman, K.A., Schmidt, M.O., Ma, X., Kabbara, K.W., Uren, A., Tomita, Y., Goetz, R., Mohammadi, M., Wilcox, C.S., et al. (2018). Fibroblast Growth Factor Binding Protein 3 (FGFBP3) impacts carbohydrate and lipid metabolism. Sci. Rep. *8*, 15973.

73. Grose, R., Fantl, V., Werner, S., Chioni, A.M., Jarosz, M., Rudling, R., Cross, B., Hart, I.R., and Dickson, C. (2007). The role of fibroblast growth factor receptor 2b in skin homeostasis and cancer development. EMBO J. *26*, 1268–1278.

74. Yang, X., Zhong, X., Huang, A.J., and Reneker, L.W. (2022). Spontaneous acinar and ductal regrowth after meibomian gland atrophy induced by deletion of FGFR2 in a mouse model. Ocul. Surf. *26*, 300–309.

75. Parfitt, G.J., Lewis, P.N., Young, R.D., Richardson, A., Lyons, J.G., Di Girolamo, N., and Jester, J.V. (2016). Renewal of the Holocrine Meibomian Glands by Label-Retaining, Unipotent Epithelial Progenitors. Stem Cell Rep. *7*, 399–410.

76. Centonze, A., Lin, S., Tika, E., Sifrim, A., Fioramonti, M., Malfait, M., Song, Y., Wuidart, A., Van Herck, J., Dannau, A., et al. (2020). Heterotypic cell-cell communication regulates glandular stem cell multipotency. Nature *584*, 608–613.

77. Selleri, S., Seltmann, H., Gariboldi, S., Shirai, Y.F., Balsari, A., Zouboulis, C.C., and Rumio, C. (2006). Doxorubicin-induced alopecia is associated with sebaceous gland degeneration. J. Invest. Dermatol. *126*, 711–720.

78. Murphy, G.F., Lavker, R.M., Whitaker, D., and Korngold, R. (1991). Cytotoxic folliculitis in GvHD. Evidence of follicular stem cell injury and recovery. J. Cutan. Pathol. *18*, 309–314.

79. Landthaler, M., Kummermehr, J., Wagner, A., and Plewig, G. (1980). Inhibitory effects of 13-cis-retinoic acid on human sebaceous glands. Arch. Dermatol. Res. *269*, 297–309.

80. Goldstein, J.A., Comite, H., Mescon, H., and Pochi, P.E. (1982). Isotretinoin in the treatment of acne: histologic changes, sebum production, and clinical observations. Arch. Dermatol. *118*, 555–558.

81. Plewig, G., and Kligman, A.M. (1978). Proliferative activity of the sebaceous glands of the aged. J. Invest. Dermatol. *70*, 314–317.

82. McGinnis, C.S., Murrow, L.M., and Gartner, Z.J. (2019). DoubletFinder: Doublet Detection in Single-Cell RNA Sequencing Data Using Artificial Nearest Neighbors. Cell Syst. *8*, 329–337.e4.

83. Hao, Y., Hao, S., Andersen-Nissen, E., Mauck, W.M., 3rd, Zheng, S., Butler, A., Lee, M.J., Wilk, A.J., Darby, C., Zager, M., et al. (2021). Integrated analysis of multimodal single-cell data. Cell *184*, 3573–3587.e29.

84. Dai, M., Pei, X., and Wang, X.J. (2022). Accurate and fast cell marker gene identification with COSG. Brief. Bioinform. *23*, bbab579.

85. Bergen, V., Lange, M., Peidli, S., Wolf, F.A., and Theis, F.J. (2020). Generalizing RNA velocity to transient cell states through dynamical modeling. Nat. Biotechnol. *38*, 1408–1414.

86. Qiu, X., Hill, A., Packer, J., Lin, D., Ma, Y.A., and Trapnell, C. (2017). Single-cell mRNA quantification and differential analysis with Census. Nat. Methods *14*, 309–315.

87. Qiu, X., Mao, Q., Tang, Y., Wang, L., Chawla, R., Pliner, H.A., and Trapnell, C. (2017). Reversed graph embedding resolves complex single-cell trajectories. Nat. Methods *14*, 979–982.

88. Yu, G., Wang, L.G., Han, Y., and He, Q.Y. (2012). clusterProfiler: an R package for comparing biological themes among gene clusters. OMICS *16*, 284–287.

89. Andreatta, M., and Carmona, S.J. (2021). UCell: Robust and scalable single-cell gene signature scoring. Comput. Struct. Biotechnol. J. *19*, 3796–3798.

90. Carlson, M. (2015). Org. Mm. Eg. Db: Genome Wide Annotation for Mouse (Bioconductor). http://bioconductor.org/packages/org.Mm.eg.db/.

STAR★METHODS

KEY RESOURCES TABLE

REAGENT or RESOURCE	SOURCE	IDENTIFIER
Antibodies		
Rabbit anti-FGFR2	Cell Signaling	Cat # 23328S
Chicken anti-K14	Biolegend	Cat # 906004
Chicken anti-K5	Biolegend	Cat # 905903
Rat anti-Ki67	eBioscience	Cat # 14-5698-80
Goat anti-K79	Santa Cruz	Cat # sc-243156
Rabbit anti-PPARγ	Cell Signaling	Cat # 2443S
Rabbit anti-p44/42 (pErk1/2)	Cell Signaling	Cat # 4370
Chicken anti-GFP	Abcam	Cat # ab13970
Goat anti-Scd1	Santa Cruz	Cat # sc-14719
Biological samples		
Mouse tissue samples, obtained in accordance with guidelines established by the University of Michigan Unit for Laboratory Animal Medicine	This manuscript	Study protocol # PRO00010041
Chemicals, peptides, and recombinant proteins		
Doxycycline chow (1 g/kg)	BioServ Inc	Cat # F3949
Tamoxifen chow (400 mg/kg, irradiated)	Envigo	Cat # TD.130860
0.25% Trypsin (no EDTA)	Invitrogen	Cat # 15050065
Albumin, Bovine Fraction V (BSA)	Research Prod. International	Cat # A30075
Hank's balanced salt solution (HBSS)	Gibco	Cat # 14025092
Nair hair removal lotion	Nair	Cat # B001E6OAM8
Hematoxylin	Sigma	Cat # HHS16
DAPI	Sigma	Cat # 32670
Nile Red	Sigma	Cat # N3013
Pemigatinib (INCB054828)	SelleckChem	Cat # S0088
Calcipotriol (MC903)	Sigma	Cat # C4369
Critical commercial assays		
RNAscope 2.5 HD Reagent Kit-BROWN	ACD (RNAscope)	Cat # 322310
RNAscope 2.5 Pretreat Reagents-H202 and Protease Plus	ACD (RNAscope)	Cat # 322330
RNAscope Target Retrieval	ACD (RNAscope)	Cat # 322000
RNAscope Wash Buffer	ACD (RNAscope)	Cat # 310091
Deposited data		
Data files for single-cell RNA sequencing	This study	GEO: GSE225252
Experimental models: Organisms/strains		
Mouse: Lrig1$^{tm1.1(cre/ERT2)Rjc}$ (Lrig1-Cre^{ERT2})	The Jackson Laboratory	Cat # 018418
Mouse: B6.129-Pparg$^{tm2Rev/J}$ (Pparg-flox)	The Jackson Laboratory (by way of Dr. Y. Eugene Chen)	Cat # 004584
Mouse: B6;129-Pparg$^{tm1.1(tTA)/Jmgr}$/J (AdipoTrak)	The Jackson Laboratory	Cat # 024755
Mouse: B6.Cg-Tg(tetO-cre)1Jaw/J (TRE-Cre)	The Jackson Laboratory (by way of Dr. A. Dlugosz)	Cat # 006234
Mouse: Gt(ROSA)26Sor$^{tm1(EYFP)Cos}$ (YFP reporter)	The Jackson Laboratory	Cat # 006148
Mouse: C57BL/6J	The Jackson Laboratory	Cat # 000664
Oligonucleotides		
In situ probe: mouse Acp5	ACD (RNAscope)	Cat # 465001
In situ probe: mouse Mgst2	ACD (RNAscope)	Cat # 819931

(*Continued on next page*)

Continued		
REAGENT or RESOURCE	SOURCE	IDENTIFIER
In situ probe: mouse Awat1	ACD (RNAscope)	Cat # 1172821-C1
In situ probe: mouse Slc6a19	ACD (RNAscope)	Cat # 897821
In situ probe: mouse Pparg	ACD (RNAscope)	Cat # 418821
In situ probe: mouse Krt79	ACD (RNAscope)	Cat # 436201
Software and algorithms		
Cell Ranger v6.1.2	10X Genomics	https://support.10xgenomics.com/single-cell-gene-expression/software/pipelines/latest/installation
DoubletFinder v2.0	McGinnis et al.[82]	https://github.com/chris-mcginnis-ucsf/DoubletFinder
Seurat v4.3.0	Hao et al.[83]	https://github.com/satijalab/seurat
COSG v0.9.0	Dai et al.[84]	https://github.com/genecell/COSGR
scVelo v0.2.5	Bergen et al.[85]	https://github.com/theislab/scvelo
Monocle 2	Qiu et al.[86,87]	https://github.com/cole-trapnell-lab/monocle2-rge-paper
clusterProfiler v4.6.0	Yu et al.[88]	https://github.com/YuLab-SMU/clusterProfiler
UCell 2.2.0	Andreatta and Carmona[89]	https://github.com/carmonalab/UCell
R	R Core	https://www.r-project.org/
Python	Python Software Foundation	https://www.python.org/
org.Mm.eg.db	Carlson[90]	http://bioconductor.org/packages/org.Mm.eg.db/

RESOURCE AVAILABILITY

Lead contact

Further information and requests for resources and reagents should be directed to and will be fulfilled by the lead contact, Sunny Wong (sunnyw@umich.edu).

Materials availability

All reagents generated in this study are available from the lead contact.

Data and code availability

- Single cell RNA sequencing data generated for this study have been deposited in the GEO database: https://www.ncbi.nlm.nih.gov/geo/query/acc.cgi?acc=GSE225252.
- This paper does not report original code.
- Any additional information required to reanalyze the data reported in this work is available from the lead contact upon request.

EXPERIMENTAL MODEL AND STUDY PARTICIPANT DETAILS

Animals

For labeling studies, PPARγ;YFP mice were fed doxycycline-containing chow (1 g/kg, BioServ Inc, F3949) *ad libitum* to suppress tTA activity, starting at 8 weeks of age, unless otherwise indicated in the text. For SG ablation and regeneration studies, LP mice and Cre-negative littermate controls were fed irradiated TAM-containing chow (400 mg/kg, Envigo TD.130860) starting at either 6 or 8 weeks of age, as indicated in the text. Pemigatinib (INCB054828, SelleckChem) was dissolved in DMSO to a stock concentration of 4 mg/mL, then subsequently diluted in PEG 400/5% dextrose in water (75:25 v/v). Mice were treated daily at a dose of 1 mg/kg body weight by oral gavage for 14 consecutive days after depilation during the chase period. To assess Lrig1-CreERT2-mediated recombination, Lrig1-CreERT2;ROSA-YFP mice were fed TAM-containing chow starting at 8 weeks of age for 5 continuous weeks. PPARγ;YFP, LP, Cre-negative littermate control and Lrig1-CreERT2;ROSA-YFP mice were of a mixed genetic background, and both genders were analyzed in roughly equal numbers for experiments. Calcipotriol (C4369, Sigma) was dissolved in 100% ethanol and 5.3 nmols were applied topically onto shaved skin for 9 consecutive days at a volume of 200 μL, then harvested 1 day after the final

treatment. For calcipotriol, IHC and RNAscope characterization studies, staining was performed on skin from C57BL/6 mice of both genders, 8-10 week of age, unless otherwise indicated in the text.

METHOD DETAILS

Whole mount analysis

Whole mounts of telogen dorsal skin were performed as previously described.[20] Briefly, skin was shaved, excised, stretched on a paper towel, covered with Elmer's No-Wrinkle rubber cement and overlayed with cellophane tape. Following incubation for 6 hours in 5 mM EDTA/PBS at 37°C, the epidermis was separated from the dermis and fixed in formalin for 30 minutes at room temperature. Finally, the samples were incubated with Nile Red (4 μg/ml) and DAPI (1 μg/ml) for 30 min in PBS with gentle agitation at room temperature, then mounted with Vectashield on a microscope slide and imaged.

Flow cytometry

Label-on PPARγ;YFP mice were euthanized at 8 weeks of age, and dorsal skin was shaved and removed. The epidermis was separated from the dermis and cell suspensions were obtained by overnight trypsinization (0.25% trypsin, Invitrogen) at 4°C, as previously described.[43] Single cells were resuspended in 2% BSA/HBSS, stained with DAPI to exclude dead cells, and sorted using a SH800 cell sorter (Sony). For scRNA-seq, 60,000 YFP+ cells from an 8 week-old PPARγ;YFP label-on male mouse were sorted into 300 μL of 2% BSA/HBSS buffer, at a ratio of 3:1 FSC/BSC-high:FSC/BSC-low, where "high" cells represented the largest ~10% of cells by FSC/BSC, and "low" cells comprised the remaining 90% by FSC/BSC (Figure 3A). For visualizing sebocytes, cells were sorted into PBS, stained with Nile Red and DAPI without fixation, and imaged.

Single cell library preparation

Single cell suspensions were subjected to counting on the LUNA Fx7 Automated Cell Counter (Logos Biosystems) and diluted to a concentration of 300 cells/μL. Single nuclei 3′ Gene Expression LT libraries were generated using the 10x Genomics Chromium instrument following the manufacturer's protocol (Chromium Next GEM Single Cell 3′ LT Kit v3.1). In brief, suspensions were loaded onto the 10x chip along with reverse transcription (RT) master mix and appropriate gel beads. Following generation of single-cell gel bead-in-emulsions (GEMs), reverse transcription was performed, and the resulting Post GEM-RT product was cleaned up and the cDNA was amplified. cDNA was subjected to enzymatic fragmentation and size selection to optimize the cDNA size prior to final library construction following the manufacturer's protocol (10x Genomics). Final library quality was assessed using the LabChip GX (PerkinElmer). Libraries were then subjected to paired-end sequencing according to manufacturer's protocol (Illumina NovaSeq 6000). Four LT reactions were run in parallel (LT1-4) from the same animal.

Single cell data processing and analysis

Bcl2fastq2 Conversion Software (Illumina) was used to generate de-multiplexed fastq files, and the CellRanger Pipeline (10x Genomics) was used to align reads and generate count matrices against the mouse genome GRCm38/mm10. For downstream analysis, the Seurat (v4.3.0) R package[83] was used to combine the 4 cell libraries and a merged Seurat object was generated. Genes detected in <3 cells were removed. Low-quality cells were further filtered on the basis of total UMI counts per cell (>900 and <80,000), number of detected genes (>200 and <7,000) and mitochondrial genes fraction (<15%). Applying these filters resulted in a final dataset of 1,066 single cell transcriptomes (Figures S6A and S6B).

To account for batch effects, the merged Seurat object was normalized using the NormalizeData() function with a scale factor of 10,000, and variable features were identified using FindVariableFeatures() with 2,000 genes. Principal component analysis (PCA) was used and the first 30 principal components (PCs) were further summarized using UMAP dimensionality reduction. We chose to use 30 PCs based on results from analyses using Elbow plots. Clustering was conducted using the FindNeighbors() and FindClusters() functions using 30 PCA components and a resolution parameter set to 0.7. A library-split UMAP plot was generated by DimPlot() function to evaluate inter-sample differences. For batch effect detection across different libraries, the distribution of the first principal component (PC1) obtained after PCA analysis was visualized by VlnPlot(). As no obvious batch effect was observed between samples (Figures S6C–S6E), we utilized the processed merged Seurat object for subsequent analysis.

For potential doublet detection, we identified doublets with DoubletFinder (v2.0).[82] The doublets were predicted using the cleaned pre-processed merged Seurat data. We did not filter doublets because no discrete doublet-enriched cluster was identified, and only few doublets were observed in the dataset.

Cluster markers were interpreted and assigned using established cell type annotations: *Krt5*/*Krt1*(+), *Lrig1*(-) and *Pparg*(-) for blended interfollicular epidermis (IFE); *Defb6*(+), *Cst6*(+), *Krt17*(+) and *Krt79*(+) for mixed upper hair follicle cells (uHF); *Krt5*(+), *Krt14*(+), *Lrig1*(+) and *Pparg*(-) for SG basal cells (BAS); *Krt5*(+) and *Pparg*(+) for transitional basal cells (t-BAS); and *Cidea*(+), *Scd1*(+) and *Fasn*(+) for differentiated sebocytes (SEB1/2/3). Absence of non-epithelial cell lineages was confirmed by assessing canonical markers, including *Pecam1*, *Cdh5* (endothelial); *Pdgfra*, *Col1a1*, *Col3a1* (fibroblast); *Ptprc*, *Cd52* (immune); *Adipoq* (adipocyte); *Pmel*, *Mlana* (melanocyte); and others.

To assess the effects of cell cycle heterogeneity on cell clustering, cell cycle phase scores were estimated using Seurat's CellCycleScoring function with mouse homologs of the cell cycle gene sets provided by Seurat. No obvious clustering differences

were found between G2M and S phases within differentiating cells (Figures S7A and S7B). The signals separating non-cycling cells and cycling cells were also checked by combined G2M and S phase gene scoring (cycling cell scoring) and showed high correlation between cycling cell score and corresponding cell states (Figure S7C).

To identify DEGs in each cell cluster, we used the Seurat FindAllMarkers function and the COSG (v0.9.0) R package[84] (Figure S2). The COSG-identified top genes were used to establish the cell identity of each cluster, along with markers described in the literature for assigned cell states. Gene signature scores were calculated on the basis of the scRNA-seq data. For each gene signature, individual cells were scored using UCell (v2.2.0) R package[89] and projected onto UMAP plots (Figure S7D).

scVelo (v.0.2.5)[85] and Monocle 2[86,87] were used for trajectory analysis. For scVelo, reads that passed quality control after clustering were used as input for the velocyto command line. The mouse expressed repeat annotation file was retrieved from UCSC genome browser. The genome annotation file was provided by CellRanger. The output loom file was used as input to estimate velocity. Velocity embedding was estimated using either the steady-state or likelihood-based dynamical model. PAGA was performed using the sc.tl.paga function in scVelo. For Monocle 2, we built a new CellDataSet object from the cluster-annotated Seurat object using the newCellDataSet function. We used the differentialGeneTest function to derive DEGs from each cluster, and genes with $q < 1 \times 10^{-4}$ were used to order cells in pseudotime. Dimension reduction was performed using the DDRTree algorithm and cells were ordered along the trajectory.

Gene Ontology enrichment analysis was performed using clusterProfiler.[88] bitr() was first employed to map gene symbols to Entrez IDs using org.Mm.eg.db (v3.16.0)[90] as the reference database, and then the enrichGO function was used with "ont = "BP", pAdjustMethod = "BH", pvalueCutoff = 0.01, and qvalueCutoff = 0.05".

Immunohistochemistry and RNAscope

Frozen sections were probed with antibodies against the following antigens: FGFR2 (1:1000), GFP (1:1000), Ki67 (1:300), K14 (1:1000), K5 (1:1000), K79 (1:400), p44/p42 (1:100), PPARγ (1:300) and Scd1 (1:300). In some cases, fluorescent images were processed using the Auto-Blend feature of Adobe Photoshop CS6 to automatically maximize image sharpness across multiple focal planes. RNAscope 2.5 Brown kit (ACD Bio) was used for RNA *in situ* staining according to manufacture's protocol. After deparaffinization, 5 μm sections were boiled for 15 minutes in RNAscope retrieval buffer, treated with protease for 30 minutes and incubated with target probes for 2 hours at 40°C. Probe detection was performed according to manufacturer's instructions.

QUANTIFICATION AND STATISTICAL ANALYSIS

SG quantitation

All analyses utilized a minimum of 4 mice per genotype ($\geq$ 2 per gender) and timepoint. Experiments utilized matched mutant and control litter-mate animals, whenever possible. To quantitate SGs in whole mounts, 2 representative fields at 5x magnification were photographed for DAPI and Nile Red staining, and subsequently all images were divided into thirds by drawing guide lines. SG presence or absence was scored for every third hair follicle that intersected these guide lines, yielding 18-25 randomly selected follicles per field. To quantitate SGs from sections, frozen skin sections (8 μm) were stained with antibodies against PPARγ and Scd1. The number of PPARγ/Scd1 double-positive SG clusters was then counted and normalized to the length of the skin section.

Statistics

SG quantitation data are depicted as means from independent biological replicates. Unpaired t tests were performed in most cases to determine statistical significance. For matched samples harvested from the same animal, paired t tests were used for comparisons between groups. Error bars are depicted as SEM.